Mitophagy-related prohibitin 2 is an orthoflavivirus restriction factor targeted for degradation during infection

Imanol Rodrigo[1,2,3¶], María José Romero de Ávila[1,2,3¶], Belén García-Navarro[1,2,3], Martín Arellano[1,2,3], Laura Albentosa-González[1,2,3,4], Pilar Clemente-Casares[1,2,3,4], Edward Emmott[5*], Armando Arias[1,2,3,6*]

Affiliations:

[1]Unidad de Medicina Molecular, Instituto de Biomedicina de UCLM (IB-UCLM), Universidad de Castilla-La Mancha (UCLM), Albacete, Spain.

[2]Unidad de Biomedicina UCLM-CSIC, Albacete, Spain.

[3]Instituto de Investigación Sanitaria de Castilla-La Mancha (IDISCAM), Spain.

[4]Facultad de Farmacia, UCLM, Albacete, Spain.

[5]Centre for Proteome Research, Department of Biochemistry, Cell & Systems Biology, Institute of Systems, Molecular & Integrative Biology, Biosciences Building, Crown Street, University of Liverpool, Liverpool, L69 7ZB, United Kingdom.

[6]Escuela Técnica Superior de Ingenieros Agrónomos y de Montes y Biotecnología (ETSIAMB), UCLM, Albacete, Spain.

Running title: Prohibitin 2 restricts orthoflaviviral replication

* Address correspondence to:

Armando Arias, armando.arias@uclm.es; Edward Emmott, e.emmott@liverpool.ac.uk

¶ These authors equally contribute to this work

Keywords: Zika, Usutu, host-virus interactions, NS5 polymerase, NS2B/NS3 protease, LGALS3BP, myoferlin, restriction factors, proviral factors.

1. ABSTRACT

Mitophagy selectively removes depolarised and damaged mitochondria, promoting cell viability. Some members of the *Orthoflavivirus* genus activate mitophagy to allow extended replication times in a surviving cell, while others inhibit mitophagy to favour viral spread. Viral genome replication is catalysed by non-structural protein 5 (NS5), the largest and most conserved protein in the orthoflaviviruses (OFVs). Here, we used quantitative proteomics to identify host cell interactors of Zika virus (ZIKV), Usutu virus (USUV), and West Nile virus (WNV) NS5 proteins. A total of 141 cellular interactors were found, of which 26 were common to all three NS5s. RNA interference (RNAi)-mediated knockdown of those proteins most significantly enriched revealed putative proviral and restriction activities associated. Knockdown of host myoferlin and LGALS3BP led to decreases in the virus titres, suggesting that both positively promote viral replication. Silencing of mitophagy-related prohibitin 2 (PHB2) resulted in significant increases in ZIKV and USUV titres, as well as intracellular levels of genomic RNA. Supporting a connection between this antiviral behaviour and mitophagy, an inhibitor of this pathway also led to larger virus titres and genomic viral RNA. During an infection, PHB2 protein levels gradually decreased, becoming transiently undetectable, and suggesting that it is specifically targeted and degraded by virus-mediated activities. Ectopic expression of NS5 alone did not affect PHB2 intracellular abundance, however a significant decrease was observed in cells expressing the viral protease NS2B/NS3. Its elimination, however, was more pronounced in cells where both viral enzymes were co-expressed, suggesting that NS5 could be assisting PHB2 recognition by NS2B/NS3. Overall, our results support that PHB2 is an orthoflaviviral restriction factor which is targeted for degradation to favour viral replication.

2. AUTHOR SUMMARY

Orthoflaviviruses (OFVs) are one of the leading causes of disease transmitted by mosquitoes, with millions of infections annually, and large numbers of deaths and cases of severe disease associated. Some important members of this group include viruses causing dengue, yellow and West Nile fevers, and Zika-associated disease (e.g. microcephaly). OFVs contain a genome which is copied by a highly conserved viral protein termed NS5. Prohibitin 2 (PHB2) is a multitasking host protein involved in different cellular processes including mitophagy, a mechanism to remove damaged mitochondria, modulate inflammation and maintain cellular homeostasis. Here, we show that human PHB2 interacts with the viral NS5 of diverse orthoflaviviruses. Depletion of PHB2 results in increased viral replication, suggesting that this protein is a restriction factor for viral infection. We found that during infection PHB2 is targeted for degradation by the viral protease, namely NS2B/NS3, in a process aided by NS5. These results support that several viral proteins act in a coordinated manner to eliminate PHB2, counteracting its antiviral activity, and thus favouring virus infection progress.

3. INTRODUCTION

Over 50 per cent of the entire human population is at risk of infection by different members of the *Orthoflavivirus* genus [1–3]. Most human orthoflaviviruses (OFVs) are transmitted by mosquitoes, with estimates suggesting that ~400 million people get infected annually, leading to >100,000 associated deaths [4,5]. The economic burden of Zika virus (ZIKV) and dengue virus (DENV) infections combined exceeds 3 billion USD annually, and 80 billion since 1975 [6]. Global warming and a broader geographic dissemination of competent vectors, among others, are factors contributing to a steady increase in the incidence and expansion of orthoflaviviral disease [4]. During the last decade, ZIKV was declared a human pathogen of international concern following large epidemic outbreaks that primarily affected the Americas and several countries in Southeast Asia. Now, the virus is present in more than 80 countries, with locally acquired cases recently documented in the EU, and estimates suggesting that 10-100 million people have been infected since the beginning of ZIKV epidemics [7–9]. Sequelae associated with infection during pregnancy can lead to severe congenital malformations, such as microcephaly, which is the most common syndrome [10]. Although generally asymptomatic, infection in adults can cause clinical manifestations of different degree of severity, such as rash, arthralgia, conjunctivitis, meningitis, encephalitis and the Guillain-Barré syndrome [11,12].

OFVs infecting birds as their natural vertebrate hosts are an additional source of public health concern [13]. Even though humans are typically dead-end hosts for avian OFVs, neuroinvasive infection leading to severe disease occur in a significant number of cases. West Nile virus (WNV) is the most relevant avian OFV from a public health perspective, with infections in North America and Europe resulting in thousands of cases of severe disease and hundreds of fatalities annually [14]. Similarly to ZIKV, WNV infection is generally asymptomatic or leads to mild-febrile illness, but one of each 100 cases results

in serious neuroinvasive disorders [15]. Usutu virus (USUV) constitutes a new emerging orthoflaviviral threat to humans. Despite that it generally leads to milder outcomes than WNV, a gradual increase in the number of neurological disorders associated with USUV infection has been reported [16–19]. WNV and USUV are genetically similar and exhibit serological cross-reactivity, which compromises their correct diagnosis in areas where cocirculation occur. Some evidence suggests that USUV infection in humans has been historically misdiagnosed as WNV, and its true impact on public health underestimated [18,20].

The OFV genome is a positive-stranded RNA molecule which is directly translated into a single polyprotein. This polypeptide is co- and post-translationally processed by both cellular activities and the viral NS2B/NS3 protease, resulting in the release of different mature structural and non-structural proteins [21,22]. Non-structural protein 5 (NS5) contains two enzymatic activities which are critical to viral genome replication. The RNA-dependent RNA polymerase (RdRp) domain, located in the C-terminal region, synthesises new viral RNA genome copies, whereas the N-terminal methyltransferase (MTase) domain catalyses the O- and N-methylation capping of the genomic 5’ end, then required for viral RNA translation and evasion of innate immunity responses [23]. OFV replication factories are assembled inside partially secluded invaginations on the endoplasmic reticulum (ER) membranes while allowing the recruitment of cellular factors that are critical for the replication process [24–26]. These substructures ensure that replicating viral RNA is isolated from host cytoplasmic antiviral sensors. In addition to non-structural viral proteins, forty-six cellular factors have been recently identified inside these replication vesicles, most of them displaying proviral activities [24].

The use of small molecule compounds against host cell proteins necessary for viral

replication has emerged as an attractive field in antiviral research [27,28]. In addition to its central activity in genome replication, NS5 has been revealed as a multifaceted protein, engaging in diverse processes that include suppression of innate immunity, transcription reprogramming, and interference with normal cell cycle progression [29–31]. Several NS5 cellular partners have already been identified, including proviral activities [24,28,32–35] and restriction factors, such as those in the JAK-STAT pathway [36–38].

Mitophagy is a type of selective autophagy to remove irreparably damaged or depolarised mitochondria and promote cell survival. Since damaged mitochondria can activate innate immunity and proinflammatory responses, many viruses modulate mitophagy in an infected cell [39]. When this pathway is activated, PINK1 is accumulated in the outer mitochondrial membrane (OMM), leading to the recruitment of E3-ubiquitin ligase Parkin [40]. Parkin ubiquitylates different OMM proteins, attracting other factors needed to initiate mitophagy [41]. The mitochondrial fusion-fission cycle is critical to this cellular process, since impaired fission blocks mitophagy activation [42]. Prohibitin 2 (PHB2), a multitasking protein found in several subcellular locations, has been recently identified as a mitophagy receptor [40,43]. PHB2 interacts with SQSTM1 and LC3 in the inner mitochondrial membrane to drive damaged mitochondria to the autophagosome [44].

Evidence support that mitophagy is actively modulated by OFVs during infection [45]. The activation of mitophagy is necessary for Japanese encephalitis virus (JEV) replication in a hepatoma cell line [46]. Mitophagy activation also exhibits a positive effect on the establishment of a persistent infection by hepatitis C virus (HCV), closely related to the OFVs [47]. Mitophagy is however silenced during DENV infection, leading to an accumulation of damaged mitochondria and cellular injury [48]. For ZIKV, mitophagy activation has been associated with both proviral and antiviral activities [45]. Ponia and

colleagues demonstrated that ZIKV supresses mitophagy in astrocytes, in a process where NS5 interacts and interferes with host protein Ajuba [49]. While no overall effect was observed on viraemia, Ajuba knockout (KO) mice showed larger viral loads in tissues, and also an increase in proinflammatory cytokines and interferon β (IFN-β), supporting that mitophagy inhibition and enhanced inflammatory responses promote virus dissemination [49]. By contrast, Lee and Shin found that mitophagy inhibition, through RNAi-mediated PINK1 silencing, repressed viral replication, suggesting that mitophagy is distinctly regulated by different OFVs and/or cellular contexts to maximise virus infection and propagation [45,50].

In the present study, we identified 141 host factors that interact with the NS5 proteins of ZIKV, WNV, and USUV. We found that 26 of these factors were common interactors for all three NS5s, including PHB2. PHB2 gene silencing led to increases in both virus titres and genomic RNA, supporting that this protein may act as a restriction factor. During both ZIKV and USUV infection, PHB2 abundance gradually decreased, becoming transiently undetectable in the infected cultures, and supporting that OFVs specifically target PHB2 to promote viral replication. Ectopic expression of NS2B/NS3 protease but not NS5 led to PHB2 degradation. PHB2 was eliminated more efficiently by NS2B/NS3 when NS5 was co-expressed in the same cells, supporting that NS5 may be assisting the viral protease in the recognition and subsequent degradation of PHB2. In the study, we identified other NS5 interactors that were critical to virus infection, such as myoferlin (MYOF) and LGALS3BP, encouraging the use of specific drugs as potential therapeutics.

4. MATERIALS AND METHODS

4.1. Cells, viruses, and protocols for infections

The origin of ZIKV and USUV strains has been detailed in previous manuscripts [33,51,52]. For virus infections, A549 (adenocarcinoma human alveolar line), Huh7.5 (human hepatoma line), HEK 293T (human embryonic kidney cells expressing SV40 T-antigen), and Vero (African green monkey kidney epithelial line) cells were used as previously described [33,53]. All the cells were grown in complete media containing either 5% (Vero) or 10% (293T, Huh7.5, A549) (v/v) foetal bovine serum (FBS, Sigma or Cytiva) and 100 units/ml penicillin-streptomycin (Gibco) in high-glucose DMEM (Gibco). Huh7.5, A549 or 293T cells media were supplemented with 2 mM L-glutamine (Gibco). Vero cells media contained 1 mM HEPES pH 7.0.

Infections were carried out as described in previous manuscripts [33,54]. Briefly, the day before virus inoculation 2 x 10^4 or 1 x 10^5 cells were seeded in either 96-well or 24-well plates, respectively, in the presence of complete media, and incubated overnight at 37°C with 5% CO_2. On the next day, cell supernatants were removed and replaced with high-glucose DMEM containing 1% FBS and 100 units/ml penicillin-streptomycin. Virus was applied at the multiplicity of infection (MOI) indicated, and adsorption allowed for 1 hour. The inoculum was removed, and the cells washed to eliminate unattached virus. Cells were then covered in media containing 1% FBS. The supernatants and/or cell lysates were collected at different time points for subsequent virus titration by 50% tissue culture infectious dose ($TCID_{50}$) assays, RNA extraction and quantification (qPCR) or Western blot analysis.

4.2. Virus titration assays

Viral samples were titrated by $TCID_{50}$ assays, using protocols that have been previously described [32,33,51]. To this, 10^4 Vero cells in 60 µl of media containing 5% FBS were seeded into 96-well plate wells. On the next day, 100 µl of 10-fold serial dilutions of each

virus in media containing 1% FBS were applied to wells, reaching a final volume of 160 µl. The virus titres were determined at day 4 (USUV) or 5 (ZIKV) post-infection (pi) by scoring the number of infected wells showing apparent cytopathic effect [55,56].

4.3. Gene silencing with Dicer-substrate small-interfering RNAs (DsiRNAs)

To achieve specific host gene silencing, we used DsiRNA duplexes purchased from Integrated DNA Technologies (IDT). Information regarding the host gene-target sequence has been provided as supporting information (S1 Table). As a negative control, a DsiRNA with no human genome target, namely NonSP, was used. To specifically silence each host factor, 5 pmol of each DsiRNA were added into each well of a 96-well plate, in the presence of 0.25 µl of lipofectamine RNAiMAX (Invitrogen) and 50 µl of opti-MEM (Gibco), as suggested by the manufacturers. The mix was incubated for 20 minutes to allow the formation of RNA-lipofectamine complexes, and then 1.5 x 10^4 A549 cells were seeded on top. Twenty-four hours after transfection, the cellular supernatants were removed, and virus was inoculated at an MOI of 0.1 or 1 $TCID_{50}$/cell. Following virus adsorption during 1 h at 37 °C, the inoculum was removed, cell monolayers washed, and fresh media containing 1% FBS added. Virus titres and genomic RNA levels in the supernatants and/or attached cells were determined by $TCID_{50}$ or qPCR assays as detailed elsewhere.

4.4. Drug treatment and cell viability assays

Host targeting drugs WJ460 [3-(3-(2-methoxyphenyl)-4-oxo-2-thiazolidinyl)-N-(4-phenylbutyl) benzamide] and mdivi-1 [3-(2,4-dichloro-5-methoxyphenyl)-2-mercaptoquinazolin-4(3H)-one] were purchased from MedChemExpress. The number of metabolically live cells after exposure to these compounds relative to mock-treated cultures, or after transfection with different host-targeting DsiRNA molecules relative to

negative control DsiRNAs (not recognising human sequences) were obtained by using the *CellTiterBlue* kit (Promega), as previously described [32,33].

4.5. Viral RNA extraction and quantification by quantitative PCR (qPCR)

Total RNA was extracted from whole cell monolayers grown in 96-well plates, using NZY Total RNA Isolation kit (NZYtech). To quantify ZIKV or USUV genomic RNA in the sample, we used different sense and antisense primers, and a FAM-TAMRA probe. ZIKV RNA was detected with a probe targeting the ZIKV E gene (positions 1214 to 1244), and primers spanning positions 1192 to 1208 and 1269 to 1246, while USUV RNA was quantified using a probe targeting USUV NS1 gene (positions 3322 to 3345), and primers spanning positions 3288 to 3309 and 3372 to 3351, all purchased from IDT. To amplify and detect both ZIKV and USUV genomic RNA, we used NZYSupreme One-step RT-qPCR Probe Master Mix (2x), ROX kit (NZYtech), and RT-PCR conditions as indicated by the manufacturer, with a reverse-transcription step (15 min at 50ºC), followed by 3 min of incubation at 95°C and 40 amplification cycles of 5s at 95°C and 45s at 60°C. To obtain a standard curve containing known amounts of ZIKV and USUV RNA, 4µl of whole cell RNA purified from infected cultures was reverse transcribed in 20µl final volume using SuperScript III Reverse Transcriptase (Invitrogen). Then, 3µl of cDNA were PCR-amplified using Phire Hot Start II DNA Polymerase (ThermoFisher), and primers spanning residues 949 to 967 (forward) and 1934 to 1915 (antisense) for ZIKV, and 2809 to 2829 (forward) and 3808 to 3787 (antisense) for USUV. Both forward primers included a T7 promoter preceding the ZIKV or USUV homology region. PCR amplicons were then purified, using NZY GelPure kit (NZYtech), and ligated into the PCR Blunt plasmid using the *Zero Blunt PCR cloning* kit (ThermoFisher). Linearised plasmids containing the inserts, or directly the PCR amplicons abovementioned, were in vitro transcribed with the *mMESSAGE mMACHINE T7 Transcription* kit (Ambion) following the protocols recommended by the

provider. After DNAse treatment, the RNA transcript was purified and quantitated, using a Nanodrop spectrophotometer. The standard curve samples were prepared by 1:10 serially diluting in vitro transcribed RNA (from 10^8 to 10^1 viral RNA molecules/µL) in 100 ng/µl yeast RNA.

4.6. Relative quantification of host mRNA transcripts by qPCR

To confirm host gene knockdown after DsiRNA transfection, RNA was extracted from cells, using the NZY Total RNA Isolation kit (NZYTech), as described above. Host gene mRNA levels were determined by using the *One-step NZYSpeedy RT-qPCR Green kit, ROX* kit (NZYtech) in a CFX Duet Real Time PCR instrument (BioRad) with specific primer pairs, all provided by IDT [reference numbers (Hs.PT.58.): 27059869, 19355804, 40826680, 2219540, 3098270, 40209489, 456578.g, 3838519.g, 38465792, 22859503, 22973334, 27422678.g, 40506149, 40261049]. As a reference we used primers amplifying a housekeeping gene (Hs.PT.39a.22214836 for GAPDH). The efficiency of each transcript downregulation was calculated following the $2^{-\Delta\Delta CT}$ method [33,57]. To the detection of IFN-β overexpression in experiments involving virus-infected or poly I:C-stimulated cells, a primer set from IDT to detect host IFNB1 mRNA transcript was also purchased (Hs.PT.58.39481063.g).

4.7. Poly I:C treatment and detection of IFN-β overexpression

To analyse the effect of PHB2 downregulation on IFN-β expression, A549 cells were transfected with different amounts of poly I:C [Poly (I:C) (LMW), Invivogen], using Lipofectamine 3000 in the absence of the P3000 reagent (Invitrogen). Twenty-four hours prior poly I:C stimulation, cells were transfected with DsiRNAs (either targeting PHB2 or a control sequence with no target on the human genome), as explained above. Poly I:C-

stimulated cells were then collected at different intervals, and total cell RNA extracted as mentioned above, to analyse IFN-β gene transcription along time (relative IFNB1 mRNA).

4.8. Vectors and mutagenesis

To the expression of ZIKV, USUV, and WNV polymerases in mammalian cells we are using constructs previously prepared in our group [32,58]. Specifically, HA-tagged versions of the full NS5 protein (HA-NS5) or the RdRp domain alone (HA-RdRp) from each OFV were inserted into a pcDNA3 vector [32,33]. A vector expressing ZIKV RdRp domain (amino acids 267 to C-t) fused to an HA tag and EYFP in its N- and C-termini (pZIKV-HA-RdRp-EYFP), respectively, was also prepared. To this, the RdRp domain of ZIKV NS5 (fused to an N-terminal HA tag) was PCR shuffled with the EYFP gene from pEYFP-N1 (Clontech), including a 5x Gly linker between both sequences. The amplicon was then cloned into pcDNA3, using EcoRI and XhoI restriction sites.

To the expression of ZIKV NS2B/NS3 protease, we swapped the HA-RdRp-EYFP coding region in the plasmid mentioned above (pZIKV-HA-RdRp-EYFP) by the corresponding NS2B3-coding region, using the *In-Fusion HD EcoDry Cloning Kit* (Takara Bio). To this, the vector was first amplified with a specific reverse primer 5'-AGCGTAATCTGGAACATCGTATGGGTA-3', located immediately before the gene insert but including the HA-tag region, and a forward primer 5'-GATAACTCGAGCATGCATCTAGAG-3', spanning the region located immediately after the gene insert and a Stop codon. This resulted in the amplification of the linearised vectors devoid of any insert, but including the sequence for an N-terminal HA tag. To the amplification of the NS2B3 coding region we used a forward primer spanning ZIKV genomic positions 4224 to 4244 and a reverse primer complementary to positions 6464 to 6444. Both primers contained 15-nt tails overlapping with the linear amplicon generated

above. Both vector and NS2B3 amplicons were ligated by recombination, leading to the pZIKV-NS2B3 plasmid.

The presence of the correct expression cassette in both pZIKV-HA-RdRp-EYFP and pZIKV-NS2B3 was confirmed by Sanger sequencing. All plasmids used in this study have been transfected into HEK 293T, A549 or Huh7.5 cells with either the *Lipofectamine 3000 kit* (Invitrogen) or the *FuGENE 4K* reagent (Promega), using the instructions provided by the manufacturers.

4.9. Co-immunoprecipitation and mass spectrometry methods

HEK 293T or A549 cells were lipofected with plasmids expressing full-length ZIKV, USUV or WNV NS5 proteins (HA-NS5) or their RdRp domains (HA-RdRp or HA-RdRp-EYFP). At 24 to 48 h post-transfection, cells were scrapped on ice-cold PBS, and spun at 300x *g* for 5 min, washed in PBS twice, and the pellet resuspended at 4°C in 450 µl of RIPA buffer (10 mM Tris-HCl pH 7.5; 150 mM NaCl; 0.5 mM EDTA; 1% SDS; 1% Triton X-100; 1% deoxycholate) in the presence of 1x protease inhibitor cocktail (Complete Mini EDTA-free protease inhibitor cocktail, Merck) and 250 U/ml benzonase (Sigma). To remove the cellular debris, the lysate was then spun during 10 mins at 15000x *g* and the resulting supernatant was recovered. To ensure that each co-IP assay contained the same amount of lysate, protein concentration in each sample was determined with the *BCA Protein Assay Kit* (Pierce) and then normalised to a final volume of 400 µl in RIPA buffer. The samples were then equilibrated in 1.5 volumes (600 µl) of dilution buffer (10 mM Tris-HCl pH 7.5; 150 mM NaCl; 0.5 mM EDTA). Anti-GFP agarose beads (*protag-HiPur GFP*, Progen) or anti-HA agarose or magnetic beads (Pierce) were pre-equilibrated in 1x dilution buffer, and then added to the lysates. The mix was incubated in a rotary shaker overnight at 4ºC. The beads were then either magnetically separated (magnetic beads) or pelleted

by centrifugation (agarose beads), the supernatant eliminated, and then washed four times in wash buffer (1x dilution buffer containing 0.05% Nonidet P40 substitute, Fluka BioChemika). Finally, the co-IP proteins were released by resuspending the beads in 1x Bolt LDS Sample Buffer (Life Technologies), 1x RIPA buffer, and boiling at 90°C for 5 min.

For the identification of host cell interactors by mass spectrometry, full-length versions of ZIKV, USUV and WNV NS5 proteins were expressed in A549 cells followed by co-immunoprecipitation (co-IP), using anti-HA magnetic beads, as described above. The pulldowns were SP3-precipitated [59], trypsin digested and labelled with TMTpro. LC-MS/MS was performed on a Dionex U3000 UHPLC, in-line with a Q-Exactive-HF mass spectrometer as described previously [60]. Data were analysed with MaxQuant 1.6.7.0 [61]. N-terminal protein acetylation and methionine were set as variable modifications, enzyme specificity was set to trypsin with up to two missed cleavages. Data were searched against fasta files containing the Swissprot human proteome entries (20,300 entries, downloaded 2020/03/12) and a custom fasta file containing the HA-tagged NS5 sequences. For each NS5, four independent transfections, co-IPs were performed, one control was removed at the data analysis stage as an outlier (S1 Fig). To identify those factors that were significantly enriched in the IPs, four independent plates were mock-transfected in parallel with an empty vector (pcDNA3). NS5-interacting factors were identified using the *Perseus software* version 2.0.6.0., as previously described [62]. A list with all host factors that are significantly enriched in ZIKV, USUV and WNV HA-NS5 co-IPs followed by TMT-based proteomics are provided as supporting material (S2 – S4 Tables). The mass spectrometry data, including .fasta files has been submitted to proteomeXchange via the PRIDE repository and has accession number PXD071636.

4.10. Western blot analysis

To the detection of host and virus protein in infected cells or transient expression of recombinant cells, we followed protocols previously described [33]. Briefly, 50 µg of cell protein lysates were resolved in SDS-PAGE electrophoresis, and transferred to an Immobilon-P PVDF membrane (Millipore). The membranes were blocked in 10% non-fat dry milk in 1x Phosphate Buffered Saline (PBS) containing 0.05% Tween-20 (PBS-T) and incubated in the presence of the corresponding primary antibody (1:500 dilution in 4% non-fat dry milk), following protocols previously described [32,33]. Primary antibodies used for Western blot include mouse anti-HA epitope (BioLegend, reference 901501), rabbit anti-FLAG epitope (Proteintech, reference 20543-1-AP), rabbit anti-PHB2 (Invitrogen, PA5-21417), rabbit anti-STAT2 (Cell Signaling, 72604S), rabbit anti-ZIKV NS3 (Invitrogen, PA5-143436) and rabbit anti-ZIKV NS5 (Genetex, GTX133328). As loading controls, HRP-conjugated antibodies against GAPDH (Genetex, GTX627408-01) and tubulin (Cell Signaling, 12351S), not requiring secondary antibody to detection, were also used.

4.11. Gene ontology analysis

Gene Ontology (GO) enrichment analysis was performed on differentially abundant proteins (FDR < 0.05) in the pulldowns using g:Profiler with the Benjamini-Hochberg correction. Redundant GO Biological Process (BP) terms were reduced using rrvgo (v1.10.0) with a Wang semantic similarity threshold of 0.7. GO Cellular Component (CC) terms with <5 genes were excluded from the analysis. Remaining terms were grouped only when sub-compartments shared a parent GO category (e.g., mitochondrial compartments) and the combined gene count remained statistically robust (≥5 genes). A summary of all enrichment analysis to the identification of BP and CC terms are provided as supporting information (S5 and S6 Tables).

4.12. Statistical analysis

Statistical significance was determined using *GraphPad Prism 8* and different statistical tests as specified in each corresponding figure legend.

5. RESULTS

5.1. Identification of host factors associated with orthoflaviviral NS5s

Full-length versions of ZIKV, USUV and WNV NS5 proteins were expressed in A549 cells, and their interacting host cellular factors isolated as described in the Methods section. Mass spectrometry analyses resulted in the identification of 72, 63 and 77 cellular proteins significantly enriched in pulldowns of ZIKV, USUV and WNV NS5s, respectively (Fig 1, S1 – S4 Tables). The GO enrichment analysis revealed that most of them were either involved in biological processes that were related to the metabolism of RNA (RNA splicing and processing), ribosome biogenesis and protein translation, chromatin assembly and chromosome organisation, or aerobic respiration and proton transport in the mitochondria (Figs 1 and 2, and S2 Fig). The intersection of the three sets (ZIKV, WNV, USUV) identified 26 proteins that were found in all co-IPs (Fig 1A and S2 Fig). To the identification of those interacting factors that could be more biologically relevant to the OFVs, we re-examined the intersection, but using only the top 50 significantly enriched proteins in each pulldown. This resulted in 14 host factors present in all three sets (Fig 2, S2 – S4 Tables). Most of the host factors identified in the intersection are mitochondrial proteins (ATP5B, PHB2, PGAM5, FH and SFXN1) or participate in ribosome biogenesis and/or protein translation (RSL1D1, RPL21, RPL24, RPL24).

5.2. Silencing of NS5 host partners identifies proviral and restriction activities

To examine the biological impact of these 14 host factors to OFVs, we assessed how their silencing affected viral replication, using specific DsiRNAs against them (Fig 3). All DsiRNAs used in our study caused efficient downregulation, with over 70% reduction in each mRNA transcript compared to controls transfected with a non-specific DsiRNA (S3 Fig). Except for ribosomal proteins RPL21, RPL24 and RPL34, gene silencing had no effect or caused only a modest decrease in cell viability at 48 h post-transfection, with more than 75% live metabolically active cells for all factors studied (S4 Fig). Downregulation of either PHB2 or ribosomal L1 domain-containing protein 1 (RSL1D1) resulted in larger virus titres in the supernatant of both ZIKV- and USUV-infected cells, suggesting these two proteins are restriction factors for the OFVs (Fig 3). Downregulation of RPL21, PGAM5, SFXN1 and SMARCA5 also led to significant increases in USUV but not in ZIKV titres, while DDX21 silencing resulted in increased ZIKV but not USUV infectivity.

Silencing of LGALS3BP and MYOF significantly affected both ZIKV and USUV replication, with pronounced losses in virus titres, supporting that these are proviral proteins (Fig 3). To confirm this possibility, we examined the effect of their downregulation at different time points and MOIs, finding similar results to those obtained before (Fig 4, S5 Fig). Viral replication was significantly impaired when MYOF was silenced, with 1,000- to 10,000-fold decreases in virus titres at 72 h post-infection (hpi). MYOF downregulation modestly affected the relative amount of metabolically active cells (>80%) at 48 h post-transfection (Fig 4), supporting that the detrimental effect on viral replication is specifically related to gene silencing and not to losses in viability. Since MYOF seems to be critical to virus replication, we investigated whether it represents a suitable target for therapeutic molecules. To this, we examined the effect of a MYOF inhibitor (WJ460) on virus infection. Although WJ460 specifically inhibits all known MYOF cellular functions [63], we observed

only a modest inhibition on ZIKV titres (~1-log10 reduction), and no effect on USUV. This apparent lack of antiviral activity was observed even at concentrations causing significant cell toxicity (40 to 160 μM), in contrast to data obtained with DsiRNAs (Fig 4E – 4G).

5.3. PHB2 downregulation stimulates orthoflaviviral replication

Since the preliminary DsiRNA-based screening identified PHB2 and RSL1D1 as putative orthoflaviviral restriction factors (Fig 3), we further examined how their silencing affected virus replication (Fig 5 and S6 Fig). In agreement with our previous observations, significant increases in ZIKV and USUV titres were found at different time points and MOIs when these host genes were knocked down. Given that mitophagy modulates OFV infection, and PHB2 acts as receptor of such pathway, we further analysed the effect of this protein to the virus life cycle. We found that PHB2 silencing also led to significant increases in intracellular viral RNA in both ZIKV- and USUV-infected cells (Figs 5G – 5J). PHB2 downregulation was also accompanied with increased NS5 protein levels during ZIKV infection, further supporting that PHB2 restricts viral replication (Fig 5B and S7 Fig). To examine whether larger titres and RNA levels could be related to an increase in virus particle release, we compared extracellular to intracellular viral RNA ratios in PHB2-depleted and unspecific DsiRNA-targeted cells (S8 Fig), but no significant differences were found. This observation may indicate that larger virus titres and genomic RNA in PHB2-depleted cells may be the result of enhanced genome replication. Thus, PHB2 could be acting as an OFV antagonist, being favoured viral genome synthesis in its absence.

To assess whether the connection between PHB2 silencing and increased viral replication could be related to mitophagy, we used mdivi-1, an inhibitor of mitochondrial fission-related protein DRP1 which also represses mitophagy [64]. We confirmed that treatment with 10μM mdivi-1 resulted in both larger ZIKV titres and genomic RNA copies (Fig 6), as

observed in PHB2-downregulated cells by RNAi (Fig 5). Accordingly, larger virus titres were also detected in USUV-infected cells treated with mdivi-1 (S9 Fig).

5.4. PHB2 is transiently eliminated during infection

To further examine its biological relevance during the orthoflaviviral life cycle, we analysed PHB2 protein level kinetics in infected cultures (Fig 7). We found that PHB2 intensity gradually decreased to become barely detectable at 48 hpi (< 3% relative to mock-infected cells) in both ZIKV- and USUV-infected A549 cells (Fig 7). At later time points (60 and 72 hpi), PHB2 was again detected at intensity levels similar to those in control uninfected cells (101-145% in ZIKV and 58-69% in USUV, respectively). PHB2 signal was also transiently reduced during infection in 293T cells, supporting that this protein is specifically targeted for degradation or its expression is repressed in different human cell types (Fig 7H). No significant variations in the relative amount of PHB2 mRNA transcripts in mock- and virus-infected cells were found (S10 Fig), conveying that reduced protein levels may be due to degradation, rather than to reduced transcriptional levels. Virus titres in A549 cells plateau at 36 hpi (S10 Fig), and hence reduced PHB2 levels in the 36 to 48 hpi interval may be directly related to enhanced viral genome replication and/or particle assembly prior to release.

5.5. PHB2 depletion correlates with larger type I interferon expression in infected cells

PHB2 together with prohibitin 1 (PHB1) have been proposed as major contributors to the MAVS-mediated antiviral signalling against cytoplasmic viral RNA, leading to the activation of type I interferon (IFN-I) responses [65]. Since PHB2 is transiently eliminated during infection (Fig 7), we pondered that its degradation may be interfering with MAVS-signalling cascade. To assess this possibility, we analysed IFN-β gene (IFNB1) transcription levels in

cells where PHB2 had been previously knocked down. For both ZIKV and USUV, we found larger IFNB1 mRNA levels in PHB2-depleted cells than in cultures transfected with a non-specific DsiRNA (Figs 8A – 8D), in contrast with previous observations [65]. Since PHB2 downregulation stimulates viral replication, resulting in larger numbers of viral RNA genome copies, enhanced IFNB1 mRNA transcription could be incidental rather than directly prompted by PHB2 depletion. To evaluate this possibility, we quantitated the relative amount of IFNB1 mRNA in cells stimulated with poly I:C, a non-replicating double-stranded RNA molecule. Although modestly, we also found that PHB2 silencing resulted in significant increases in IFNB1 mRNA levels (Figs 8E – 8H). To further explore whether IFNB1 transcription activation was connected to mitophagy inhibition, we analysed mRNA levels in ZIKV-infected cells treated with mdivi-1 but, in this case, IFNB1 mRNA levels were moderately lower in the presence of the inhibitor (Fig 6D).

5.6. NS5 stimulates PHB2 degradation by the viral protease NS2B/NS3

Since host STAT2 degradation by the proteasome is directly mediated by NS5 in ZIKV and DENV [36,38], and that NS5 specifically interacts with PHB2 (Fig 2), direct PHB2 degradation by NS5 was a plausible scenario. Further supporting this possibility, ZIKV NS5 and host PHB2 protein levels coincidentally decrease at 48 hpi in A549 cells when compared to the previous data points (Figs 7A, 7C and 7D). We first confirmed that PHB2 and NS5 proteins interact in co-IP assays followed by Western blot (Fig 9A), as previously inferred from our mass spectrometry data (S2 – S4 Tables). PHB2 was also pulled down when the RdRp alone was used as a bait, supporting that NS5 interacts with this cellular protein through the polymerase domain (Fig 9B). To assess whether NS5 expression and PHB2 degradation were linked, we used increasing amounts of all three NS5 expression constructs, but no significant changes in PHB2 detection were found (Fig 9C and S11 Fig). Nonetheless, we confirmed that our ZIKV NS5 construct resulted in efficient STAT2

downregulation when transfected, as previously documented (Fig 9C and S11 Fig).

Since NS5 seemed not to be directly leading to PHB2 degradation, we anticipated that other viral factors might be involved. In addition to viral polyprotein maturation, the orthoflaviviral protease NS2B/NS3 also participates in the recognition and proteolytic cleavage of different cellular proteins during infection [66–68]. Thus, we examined the effect of ZIKV NS2B/NS3 on PHB2, confirming that the ectopic expression of its precursor (NS2B3) resulted in decreased protein levels (Fig 9D). To examine a possible synergistic activity of both viral proteins, we analysed the effect of NS5 coexpression in cells transfected with a suboptimal amount of the pZIKV-NS2B3 construct. We confirmed that the expression of viral NS2B/NS3 is accompanied by a decrease in PHB2 abundance, and that this reduction is enhanced in the presence of NS5 (Figs 9E and 9F). These observations support that both viral proteins participate in the recognition of PHB2 and its subsequent degradation.

6. DISCUSSION

Owing to its central role to the virus life cycle, here we seek to examine the interacting networks of orthoflaviviral NS5 within the host cell in full detail. We deem that this information can be instrumental in advancing our understanding on the virus-cell interactions directly engaging in viral genome replication and diverse processes affected by NS5. Mitophagy has attracted attention as a key cellular process modulating orthoflaviviral infection [49,50]. In this manuscript, we have identified PHB2, a mitophagy receptor, as a restriction factor for OFV replication. RNAi-mediated PHB2 silencing resulted in increased viral titres, genomic RNA and protein translation, sustaining our hypothesis (Fig 5). We have found that mdivi-1, a mitophagy inhibitor, also promotes higher virus titres in infected cells, supporting a relationship between this restriction activity

associated with PHB2 and this cellular pathway [64,69]. Previous studies established a connection between ZIKV NS5 and mitophagy inhibition [49]. NS5 binds to host protein Ajuba, preventing its translocation to depolarised mitochondria and supressing PINK1-mediated mitophagy activation. In our study, while a connection between PHB2 and viral replication has been established, it remains to be further examined how its degradation, observed in infected cells, affects mitophagy. In addition to PHB2, we have identified other mitochondrial proteins as NS5 interactors, such as phosphoglycerate mutase family member 5 (PGAM5) which also plays an important role during mitophagy [40,70], several subunits of the mitochondrial ATP synthase (e.g. ATP5F1B), fumarate hydratase (FH) and sideroflexin-1 (SFXN1). These findings are suggestive of mitochondria dynamics playing a crucial role during OFV infection, and of NS5 as a factor subverting some cellular processes controlled by these organelles.

Besides mitochondria, PHB2 can also be found in different subcellular locations, including the nucleus, cytosol and plasma membrane, engaging in various signalling pathways in cell metabolism, migration and proliferation [71]. A conceivable situation is that viral restriction by PHB2 is connected to other cellular processes, in addition to mitophagy. The translocation of PHB2 into the nucleus interferes with long-noncoding RNA and gene transcription, acting as a repressor of diverse transcription factors such as MyoD, MEF2 and the oestrogen receptor (ESR) [72–75]. Evidence suggests that oestrogen-dependent signalling could elicit a proviral activity, since inhibition by tamoxifen also inhibits orthoflaviviral replication [76]. Thus, a tantalising possibility is that PHB2 antiviral activity operates at the transcriptional level, and its absence exerts a proviral effect, connected to ESR-signalling activation [76–78].

PHB2 is transiently eliminated during ZIKV or USUV infection in different cell contexts, suggesting that its degradation is critical to the virus life cycle (Fig 7). Since both ZIKV and DENV NS5 proteins target STAT2 to proteasomal degradation, we initially considered that PHB2 elimination might be caused by NS5. In the case of STAT2, NS5 acts as a protein bridge between this protein and an E3 ubiquitin ligase, leading to STAT2 degradation in a ubiquitin-dependent process [36,38]. We have recently documented that OFV NS5s also interact with UBA1, the primary E1 ubiquitin-activating enzyme in most ubiquitylation events [33]. However, we found that the ectopic expression of NS5 alone does not affect PHB2 protein levels, being required the viral protease NS2B/NS3 to its degradation (Fig 9D). Nonetheless, when NS2B/NS3 is expressed at suboptimal levels, increasing amounts of NS5 are required for a gradual elimination of PHB2 (Figs 9E and 9F). A physical interaction between NS5 and the C-terminal domain of NS3 has been previously documented, and hence this could also be taking place between NS5 and the NS2B/NS3 complex [79,80]. Our current hypothesis is that NS5 facilitates the interaction between PHB2 and the viral protease, enabling its subsequent degradation. If this is correct, NS5 could be acting as a protein bridge, not only for PHB2 elimination by NS2B/NS3, but also for other restriction factors. In addition to degradation, a possible alternative is that NS5 could be sequestering PHB2 and thus interfering with other cellular processes catalysed by this protein. Several lines of evidence support that orthoflaviviral NS5s can interfere with host factors of the IFN-I-dependent JAK-STAT signalling pathway, such as IKKε and TBK1 [31,81,82].

Previous studies have established a connection between PHB2 and MAVS-mediated antiviral signalling. Therefore, a forthcoming explanation would be that OFVs targeting PHB2 to degradation might help uncouple MAVS activation from IFN-I production [65]. MAVS is activated when replicating viral RNA in the cytoplasm is detected by retinoic acid

inducible gene type I (RIG-I) – like receptors (RLRs), such as RIG-I and MDA5. Activated RLRs interact with MAVS in the mitochondrial membrane, triggering the downstream signalling pathways that lead to the production of IFN-I and proinflammatory interleukins [83,84]. Our data suggest however that PHB2 knockdown during infection activates IFN-I transcription, in contrast with previous observations [65]. We observed larger IFNB1 levels in either infected or poly I:C–stimulated cells when PHB2 was silenced (Fig 8). Yoshinaka and colleagues found that downregulation of either PHB1 or PHB2 resulted in decreased IFN-β levels after infection with Sendai virus (SeV) or poly I:C stimulation [65]. These differences could be, at least in part, attributed to the use of different cell lines, or to the fact that an infection by a positive (OFV) or a negative-stranded (SeV) RNA virus could trigger distinct responses. Further analysis is needed to better understand the possible connection between MAVS and PHB2 in the context of an orthoflaviviral infection.

Larger IFNB1 transcription levels observed in PHB2-silenced cells seems counterintuitive to the antiviral role that we are claiming for this host protein (Fig 8). This could be partially explained in the context of fluctuating PHB2 abundance observed in the infected cells. We hypothesise that transient PHB2 degradation observed at 48 hpi could be leading to enhanced viral RNA genome replication (Figs 5 and 7). Subsequent PHB2 restoration to normal levels at 60 hpi could be triggering mitophagy activation (Fig 7), thereby preventing exacerbated inflammation and hence attenuating the ensuing MAVS antiviral response against replicating viral RNA [69,85]. In agreement with this hypothesis, several studies have documented that mitophagy is critical to modulate the cellular inflammatory responses, and thus to maintain innate immunity homeostasis [86–89].

In the study we also identified other NS5 partners affecting orthoflaviviral replication. Larger virus titres were recovered in both ZIKV- and USUV-infected cells when RSL1D1

was silenced, also supporting an antiviral activity associated with this host factor (S6 Fig). RSL1D1 is an RNA-binding protein participating in multiple cellular processes, including antagonising senescence, proliferation and apoptosis, and acting as an autophagy suppressor in different types of cancer [90,91]. Conversely, MYOF and LGALS3BP downregulation led to significant decreases in both ZIKV and USUV titres, suggesting that both factors contribute to critical steps of the life cycle (Fig 4 and S4 Fig). MYOF is a multifunctional Ca2+ – binding protein which, besides vesicle trafficking regulation, participates in endocytosis-induced membrane repair activities [92,93]. Since OFVs assemble their replication sites in ER membrane invaginations requiring extensive remodelling, it is conceivable that membrane-repair activities might be relevant to their formation [94]. WJ460, a promising anticancer drug targeting MYOF Ca2+ – binding C2D domain [92,95], showed only a minor effect on virus titres, in contrast with DsiRNA-mediated silencing (Fig 4). Despite human MYOF cryo-EM structures have been recently solved, attempts to obtain a complex with WJ460 remain elusive [95]. Additional studies suggest that WJ460 may be targeting different host factors, and thus its inhibitory effects not being totally associated with MYOF [96].

LGALS3BP is a secreted glycoprotein that has been associated with immune modulation, tumour progression, and extracellular matrix organization. During infection, LGALS3BP is activated, leading to increased IFN production and proinflammatory responses [97]. WNV infection in mice results in the upregulation of LGALS3BP in the CNS [98]. However, while KO mice showed reduced neuroinflammation, increased microglial numbers, and alterations in T cell populations, no significant differences in WNV replication titres are observed [98]. This evidence suggests that LGALS3BP is not critical to WNV infection in mice, in contrast to our data with ZIKV and USUV in cell culture.

In addition to advance our understanding of the OFVs biology, we deem this study open new avenues for their therapeutic control. Approaches based on stimulating PHB2 antiviral activity or, alternatively, molecules triggering mitophagy activation, which are expected to antagonise viral replication, could be considered in future studies. The identification of the interacting epitopes between NS5 and its cellular counterparts could also be instrumental in the rational design of antivirals disrupting their binding interfaces.

7. ACKNOWLEDGEMENTS

We thank José Joaquín Lorenzo for his technical assistance to this work.

8. FUNDING INFORMATION

This research was supported by grant SBPLY/24/180225/000240, from Junta de Comunidades de Castilla-La Mancha (JCCM), awarded to AA and LAG. AA is also the recipient of grants PID2022-137974OB-I00 and CNS2022-135258 from Ministerio de Ciencia, Innovación y Universidades (MICIU/AEI/10.13039/501100011033) and FEDER (EU), and grants SBPLY/21/180501/000076 and SBPLY/24/180225/000240 from Junta de Comunidades de Castilla-La Mancha (JCCM). Work in AA's lab is also supported by core funding from UCLM (grant numbers 2025-GRIN-38349 and 2022-GRIN-34150). IR and MJRdA are, respectively, the recipients of fellowships 2020-PREDUCLM-16723 and 2024-INVGO-12348, both granted by UCLM. Research in EE's lab is supported by an AMS Springboard Award (SBF006\1008) funded by the Academy of Medical Sciences (AMS), the Wellcome Trust, the Government Department of Business, Energy and Industrial Strategy (BEIS), the British Heart Foundation and Diabetes UK, an MRC NIRG (MR/X000885/1) and Wellcome Career Development Award (227831/Z/23/Z). The funders had no role in study design, data collection and analysis, decision to publish, or preparation of the manuscript.

9. FIGURE LEGENDS

Fig 1. Summary of orthoflaviviral NS5-interacting network. (A) Overlap of host proteins interacting with different orthoflaviviral NS5 proteins (ZIKV, USUV and WNV). BioVenn was used to the graphic representation of the diagram [99]. (B) Gene Ontology analysis of cellular components (GO-CC). Related sub-compartments, i.e. mitochondrial inner membrane (GO:0005743) and mitochondrial nucleoid (GO:0042645) were grouped as 'Mitochondria' to reflect organelle-level localization. The pie chart displays the proportional distribution of significantly enriched terms (adjusted $p < 0.05$) among all factors identified in NS5-interacting datasets. (C) Heatmap of significantly enriched Gene Ontology Biological Process (GO-BP) terms in co-IPs of cells transfected with either ZIKV, USUV, or WNV HA-tagged NS5 proteins (adjusted $p < 0.05$). Each GO-BP is represented in a colour-based gradient for statistical significance [$\sqrt{(-\log_{10}}$ adjusted p-value]. GO terms were clustered hierarchically using semantic similarity (rrvgo; similarity threshold = 0.7). See S5 and S6 Tables for full terms.

Fig 2. Orthoflavivirus NS5 interaction network. Quantitative proteomics was used as described in the text to identify host factors interacting with HA-tagged versions of ZIKV, USUV or WNV NS5 proteins. Only the top 50 most significantly enriched factors in each data set are used to build the network and to identify overlaps between data sets. The protein-protein interaction network was generated using the STRING database [100]. Data clustering was generated in Cystoscape [101], using the MCL algorithm. Those factors identified in two datasets are coloured in pale yellow, and those in all three datasets in coral. Each grey-shaded area represents a cluster positively associated with a biological process (i.e. ribosome biogenesis, cytoplasmic translation, mRNA processing, chromatin organisation, proton transmembrane transport/aerobic respiration). Mitochondrial proteins

are encircled by a dotted line.

Fig 3. DsiRNA-mediated gene silencing identifies putative proviral and restriction host factors for OFV replication. Virus titres in the cellular supernatant of infected cells (n ≥ 4 biologically independent samples), previously transfected with a DsiRNA targeting an NS5-interacting factor. At 24 h post-transfection, A549 cells were infected with either ZIKV (black columns) or USUV (grey columns) at an MOI of 0.1 $TCID_{50}$/cell. Control infections were carried out in parallel experiments in cells transfected with a non-human target DsiRNA (NonSP). Relative changes in viral titres observed at 48 h postinfection in gene-silenced cultures compared to NonSP controls are shown. For clarity, the effect of host factor downregulation on viral infectivity is represented in 3 different graphs: ribosome biogenesis and translation (A), mitochondrial (B), and other ungrouped host factors (C). Significant differences observed between unspecific (NonSP) and specific host-targeting DsiRNA-transfected cells are indicated (Two-way ANOVA, Dunnett's multiple comparisons test; *, $p < 0.05$; **, $p < 0.01$; ***, $p < 0.001$). Bars are representing the standard error of the mean (SEM) for each data point.

Fig 4. Reduced virus titres in MYOF-depleted cells. (A – D) Effect of MYOF gene silencing on viral replication. (A) Relative amount of metabolically active cells after transfection with a specific (DsiMYOF) or an unspecific DsiRNA (DsiNonSP). Cell viability is determined at 48 and 72 h post-transfection as suggested in the Methods section. Values are obtained as a percentage relative to mock untransfected cells. (B) Relative MYOF mRNA expression was examined by RT-qPCR in A549 cells transfected with either a MYOF-targeting (DsiMYOF) or a non-human target DsiRNA (DsiNonSP). MYOF mRNA levels were normalised to GAPDH mRNA levels. Values obtained are the average of at least 4 independent biological replicas (n ≥ 4), and relative to untransfected cells carried

out in parallel. (C, D) Virus infectivity was examined by $TCID_{50}$ assays of samples collected at different time points from cells previously transfected with each DsiRNA. Twenty-four hours after transfection, cells were infected with ZIKV (C) or USUV (D) at an MOI of 1 $TCID_{50}$/cell. Each value in the graph is the average of ≥ 4 independent biological replicas. (E – G) Effect of MYOF-targeting drug WJ460 on ZIKV and USUV replication. (E) The relative amount of metabolically active cells after treatment during 48 h with increasing concentrations of WJ460 is calculated as indicated in (A). Values are represented as a percentage relative to mock-treated cells. (F, G) ZIKV (F) or USUV (G) titres detected in cells treated with WJ460 at 48 h postinfection. In each panel, significant differences are indicated (Two-way ANOVA, Sidak's multiple comparisons test; *, $p<0.05$; ***, $p < 0.001$). The standard error of the mean (SEM) is represented for each data point.

Fig 5. Increased viral titres, RNA and protein levels in PHB2-depleted cells. (A) Relative PHB2 mRNA expression in A549 cells previously transfected with either a PHB2-targeting (DsiPHB2) or a non-human target DsiRNA (DsiNonSP). PHB2 expression was normalised to GAPDH mRNA levels. Values obtained are the average of at least 4 independent biological replicas ($n \geq 4$), and relative to untransfected cells carried out in parallel. (B) PHB2 downregulation leads to increased ZIKV NS5 protein abundance in infected cells. Representative WB of ZIKV NS5 and PHB2 protein levels in A549 cells previously transfected with each DsiRNA and infected at 24 h post-transfection with ZIKV. As a loading reference, an anti-GAPDH antibody was used. (C – F) Virus infectivity was examined in the supernatants of cells previously transfected with each DsiRNA. Twenty-four hours after DsiRNA transfection, cells were infected with ZIKV (C, D) or USUV (E, F) at an MOI of 0.1 (C, E) or 1 $TCID_{50}$/cell (D, F). Each value in the graph is the average of four independent biological replicas ($n = 4$). (G – J) Viral RNA genome equivalents detected in samples collected at 48 hpi from cells previously transfected with each

DsiRNA. Twenty-four hours after DsiRNA transfection, cells were infected at an MOI of 0.1 or 1 $TCID_{50}$/cell with ZIKV (G, H) or USUV (I, J). Each value in the graph represents the average of viral RNA detected in four independent biological replicas (n = 4) extracted from infected cells (intracellular, graphs G and I) or the supernatant of these cultures (extracellular, graphs H and J). The statistical significance in each panel was determined by Two-way ANOVA and Sidak's multiple comparison test (C – J) or *t* (A) tests (*, $p<0.05$; **, $p<0.01$; ***, $p < 0.001$). Bars are representing the standard error of the mean (SEM).

Fig 6. Increased ZIKV titres and RNA levels in cells treated with a mitophagy inhibitor. (A) Relative number of metabolically active A549 cells after 48 hours in the presence of increasing concentrations of mdivi-1. Values are relative to untreated cells (0 μM). (B) ZIKV titres at 48 hpi in the supernatant of cells treated with increasing concentrations of mdivi-1. Cells were previously inoculated with ZIKV at an MOI of 0.1 $TCID_{50}$/cell. (C) Genomic RNA equivalents in cells infected with ZIKV, and treated with mdivi-1. D, Relative IFNB1 mRNA expression in ZIKV-infected cells treated with mdivi-1.

Fig 7. PHB2 is transiently eliminated in ZIKV- and USUV-infected cells. (A, E) Representative Western blot of PHB2 kinetics in cells infected with either ZIKV (A) or USUV (E). (B, C, F, G) PHB2 protein levels in mock- (B, F), ZIKV- (C) or USUV-infected (G) A549 cell lysates at different time points. PHB2 to tubulin band intensity ratios are relative to those obtained at 48 h in Mock-infected cultures. (D) ZIKV NS5 protein levels detected in ZIKV-infected A549 cell lysates collected at different time points. NS5 to tubulin band intensity ratios for each time point are relative to 72 hpi. Each value in the graphs is the average of three independent biological replicas (n = 3). Bars are representing the standard error of the mean (SEM) for each data point. Significant differences between mock and infected samples are indicated (One-way ANOVA; *, p <

0.05; **, $p < 0.01$). (H) Representative blot of PHB2 protein levels in 293T cells collected at different time post-infection in cells infected with ZIKV (top) or USUV (bottom). An anti-GAPDH antibody was used to calibrate total protein loading.

Fig 8. Increased IFN-I transcription in PHB2-downregulated cells. (A – D), Relative IFNB1 mRNA expression in A549 cells previously transfected with either a PHB2-targeting (DsiPHB2) or a non-human target (DsiNonSP) DsiRNA, and then infected with ZIKV (A, B) or USUV (C, D). IFNB1 expression was normalised to GAPDH mRNA levels. (E – H) Relative IFNB1 mRNA expression in A549 cells transfected with either a PHB2-targeting (DsiPHB2) or a non-human target (DsiNonSP) DsiRNA, and then stimulated with different amounts of poly I:C. IFNB1 expression was normalised to GAPDH mRNA levels. Values obtained are the average of at least 4 independent biological replicas, and relative to control cells (no DsiRNA). (E, G) IFNB1 mRNA levels in poly I:C-stimulated cells compared to control unstimulated cells. (F, H) Relative IFNB1 mRNA expression in PHB2-depleted cells compared to control cells (DsiNonSP) after poly I:C stimulation.

Fig 9. Ectopic co-expression of NS2B3 and NS5 mediates efficient PHB2 elimination. (A, B) PHB2 is co-immunoprecipitated with ZIKV, USUV and WNV NS5 proteins (A) or their RdRp domains (B). To this, 293T cells were transfected with constructs expressing HA-tagged versions of each NS5 (A), or the RdRp domain alone (B). As controls, there were included mock-transfected cells or constructs expressing EYFP (pEYFP-N1, shown as pEYFP), HA-tagged LacZ (pCruz HA-LacZ, shown as HA-LacZ) or an empty vector (pcDNA3). Cell lysates were incubated with anti-HA agarose beads binding to NS5 and RdRp, and the presence of PHB2 in the co-IPs was examined with a specific antibody. (C) ZIKV NS5 overexpression leads to reduced STAT2 but not PHB2 levels. 293T cells were transfected with increasing amounts (400, 800, 1600, 3200 ng) of either a construct

expressing HA-tagged ZIKV NS5 or an empty vector (pcDNA3). (D) Ectopic expression of NS2B/NS3 precursor (NS2B3) leads to reduced levels of PHB2 in 293T cells. To this, 5 x 10^5 293T cells were seeded on a 35-mm plate and transfected with either 2 or 4 μg of pZIKV-NS2B3 or an empty vector (pcDNA3). (E) PHB2 elimination by NS2B3 is enhanced in the presence of NS5. In this assay, 5 x 10^5 293T cells were seeded on a 35-mm plate and co-transfected with 2 μg of pZIKV-NS2B3 and 2 μg of pZIKV-HA-NS5 or an empty vector (pcDNA3). (F) Larger NS5 protein levels result in reduced PHB2 abundance in cells expressing a suboptimal amount of the NS2B/NS3 protease. Transfections were carried out upon 5 x 10^6 293T cells previously seeded on 100-mm plates. Cells were lipofected with 2 μg of pZIKV-NS2B3 and different amounts of pZIKV-HA-NS5 (gradually increasing from 0.5 to 6 μg).

10. SUPPORTING INFORMATION

S1 Fig. Quality control of the proteomic datasets. Principal component analysis (PCA) separates each coimmunoprecipitation (co-IP) dataset (n=4) from each other (ZIKV, USUV and WNV) and from control co-IP in mock-transfected cells. PCA also shows reproducible clustering of biological replicates, except for one control experiment (outlier) that has been removed for further analyses.

S2 Fig. Orthoflavivirus NS5 interaction network. Quantitative proteomics was used as described in the text to identify host factors interacting with OFV NS5 proteins. Briefly, host protein interactors were pulled down from cell lysates obtained after transfection of HA-tagged versions of ZIKV, USUV or WNV NS5 proteins and subsequent immunoprecipitation. A total of 141 proteins were identified after combining all three datasets. A protein-protein interaction network for these factors was generated using the STRING database [100]. Data visualisation was performed using Cystoscape [101], and

clustering to identify densely connected nodes was then applied to the network with the MCL algorithm. Those factors identified in two datasets were represented in pale yellow, and those in three datasets were shown in coral (only those among the top 50 most enriched factors in all three datasets) light orange (remaining host factors in all three sets). The biological process term (GO-BP) better fitting with each cluster is given.

S3 Fig. Relative knockdown efficacy of host-specific DsiRNAs in A549 cells. RT-qPCR analysis at 48 h post-transfection of host gene expression in A549 cells lipofected with a host-specific DsiRNA and normalised to GAPDH mRNA levels. Values obtained are the average of ≥ 4 independent biological replicas. Knockdown efficiency was calculated by RT-qPCR by the $2^{-\Delta\Delta Ct}$ method, using as a reference a cell culture transfected with a non-human target DsiRNA.

S4 Fig. Effect of host factor depletion on cell viability. Relative number of metabolically active cells after specific host gene downregulation. Values are relative to the fluorescence detected in mock-transfected cells. Cells were transfected with either a host factor-specific DsiRNA or an unspecific DsiRNA (NonSP). At 48 (black columns) and 72 hours post-transfection (grey columns), the relative number of viable cells (metabolically active) is calculated with the *CellTiter-Blue Cell Viability Assay kit* as suggested by the manufacturer. A dashed line is included to indicate those viability values above 70%.

S5 Fig. Reduced virus titres in LGALS3BP-depleted cells. (A) Relative amount of metabolically active cells after transfection with a specific (DsiLGALS3BP) or an unspecific DsiRNA (DsiNonSP). Values are obtained as a percentage relative to untransfected cells (not represented in the graph). (B) RT-qPCR analysis of LGALS3BP expression in A549

cells transfected with either a host-specific (DsiLGALS3BP) or a non-human target DsiRNA (DsiNonSP). LGALS3BP mRNA expression was normalised to GAPDH mRNA levels. Values obtained are the average of at least 4 independent biological replicas (n ≥ 4), and relative to untransfected cells carried out in parallel. (C, D) Virus infectivity was quantitated by $TCID_{50}$ assays in samples collected at different time points from cells previously transfected with 5 pmol of each DsiRNA, as indicated in A and B. Twenty-four hours after transfection, cells were infected with ZIKV (C) or USUV (D) at an MOI of 0.1 $TCID_{50}$/cell. Each value in the graph is the average of ≥ 4 independent biological replicas. The statistical significance was calculated by Two-way ANOVA using Sidak's multiple comparisons (A, C, D) or *t* (B) tests (*, $p<0.05$; **, $p<0.01$; ***, $p < 0.001$). Bars are representing the standard error of the mean (SEM) for each data point.

S6 Fig. Increased virus titres in RSL1D1-depleted cells. (A) Relative amount of metabolically active cells after transfection with a specific (DsiRSL1D1 or DsiPHB2) or an unspecific DsiRNA (DsiNonSP). Cell viability is determined at 48 and 72 h post-transfection as suggested in the Methods section. Values are obtained as a percentage relative to untransfected cells (not represented in the graph). (B) RT-qPCR analysis of RSL1D1 expression in A549 cells transfected with either an RSL1D1-targeting (DsiRSL1D1) or a non-human target DsiRNA (DsiNonSP). RSL1D1 mRNA expression was normalised to GAPDH mRNA levels. Values obtained are the average of 4 independent biological replicas (n=4), and relative to untransfected cells carried out in parallel. (C, D) Virus infectivity was examined in samples collected from the supernatants of cells previously transfected with each DsiRNA. Twenty-four hours after DsiRNA transfection, cells were infected with ZIKV (C) or USUV (D) at an MOI of 0.1 $TCID_{50}$/cell. Each value in the graph is the average of ≥ 4 independent biological replicas. (A – D) The statistical significance was calculated by Two-way ANOVA and Sidak's multiple

comparison test (A, C, D) or a *t* test (B) (*, $p<0.05$; **, $p<0.01$; ***, $p < 0.001$). Bars are representing the standard error of the mean (SEM) for each data point.

S7 Fig. Increased ZIKV NS5 protein levels in PHB2-depleted cells. Representative Western blot of ZIKV NS5 and PHB2 protein levels in ZIKV-infected cells previously transfected with either a specific (DsiPHB2) or a non-human target (DsiNonSP) DsiRNA. At 24 h post-transfection, ZIKV was applied to cells at an MOI of 1 $TCID_{50}$/cell. Cell lysates were collected at different time points and analysed by Western blot. As a loading reference, an anti-tubulin antibody was used. Untransfected mock-infected cells were included in the assay as a reference control.

S8 Fig. Extracellular to intracellular viral RNA levels in PHB2-downregulated cells. (A – D) A549 cells were transfected with either a non-human target (NonSP) or a PHB2-targeting DsiRNA (PHB2). At 24 hours post-transfection, cells were infected with either ZIKV (A, C) or USUV (B, D) at an MOI of 0.1 or 1 $TCID_{50}$/cell. (A, B) RT-qPCR analysis of PHB2 expression in A549 cells transfected with either a PHB2-targeting (DsiPHB2) or a non-human target DsiRNA (DsiNonSP). PHB2 mRNA expression was normalised to GAPDH mRNA levels. Values are the average of 4 independent biological replicas (n=4), and relative to controls (NonSP) for each virus, MOI and time point represented. (C, D) Ratios of extracellular to intracellular viral RNA in PHB2-depleted cells at 48 h after infection with ZIKV (C) or USUV (D). The statistical significance was calculated in each graph by Two-way ANOVA and Sidak's multiple comparisons test. Bars are representing the standard error of the mean (SEM) for each data point.

S9 Fig. Increased USUV titres in cells treated with mitophagy inhibitor mdivi-1. (A) Relative number of metabolically active A549 cells after 48 hours in the presence of

increasing concentrations of mdivi-1. (B) USUV titres in the supernatant of infected cells after treatment with increasing concentrations of mdivi-1 during 48 h. Cells were previously inoculated with USUV at an MOI of 0.1 $TCID_{50}$/cell.

S10 Fig. ZIKV and USUV replication kinetics and their effect on PHB2 and IFNB1 mRNA expression. (A) Virus titre kinetics in the supernatant of A549 cells infected with either ZIKV (black) or USUV (grey). Bars are representing the standard error of the mean (SEM) for each data point. (B) Viral genome equivalents in cells infected with ZIKV (black) or USUV (grey). (C) Relative IFNB1 mRNA levels in cells infected with ZIKV or USUV. (D) RT-qPCR analysis of PHB2 mRNA expression in A549 cells infected with ZIKV or USUV. PHB2 was normalised to GAPDH mRNA levels and expressed as relative values to mock-infected cells carried out in parallel. Values obtained are the average of ≥ 4 independent biological replicas. The statistical significance was calculated by Two-way ANOVA and Sidak's multiple comparison test (A, C, D) or a *t* test (B) (*, $p<0.05$; **, $p<0.01$; ***, $p < 0.001$).

S11 Fig. ZIKV NS5 overexpression leads to reduced STAT2 but not PHB2 protein levels. Either 1200 or 2400 ng of constructs expressing ZIKV (right panel), USUV (middle) or WNV (left) NS5 or an empty vector (pcDNA3) are transfected in 293T cells. The effect of NS5 overexpression on STAT2 and PHB2 levels are examined by Western blot. Tubulin is used as a loading control.

S1 Table. DsiRNA molecules used in the study. Nucleotide sequences of DsiRNA duplexes used for specific host gene silencing. Each DsiRNA duplex is formed by a 25-nt sense (above) and 27-nt antisense (below) RNA strand. The last two nucleotides found in

each sense strand are deoxyribonucleotides (bold typed) while the remaining are ribonucleotides. All duplexes are commercially available at IDT, except the DsiRNA for RPL21 that consequently was designed by us. Its synthesis was then requested to the same company (IDT).

S2 Table. Summary of ZIKV NS5-host protein-protein interaction networks. A list of all factors identified in the analysis, using the *Perseus* software, is included. The 50 top significantly enriched host interactors are shaded in pink. In grey, there have been highlighted the detection of HA-tagged ZIKV NS5 (correctly assigned) and USUV NS5.

S3 Table. Summary of USUV NS5-host protein-protein interaction networks. A list of all factors identified in the analysis, using *Perseus* as abovementioned, is included. The 50 top significantly enriched host interactors are shaded in pink. In grey, there have been highlighted the detection of HA-tagged USUV (correctly assigned) and WNV NS5 proteins.

S4 Table. Summary of WNV NS5-host protein-protein interaction networks. A list of all factors identified in the analysis, using *Perseus* as abovementioned, is included. The 50 top significantly enriched host interactors are shaded in pink. WNV NS5 protein identification is highlighted in grey.

S5 Table. Summary of Biological Process (BP) enrichment analysis of orthoflavivirus NS5-host protein-protein interactions. To this analysis, we used all the host factors identified in S2 – S4 Tables, and the g:GOSt application available at the g:Profiler website [102].

S6 Table. Summary of Cellular Compartments (CC) enrichment analysis of orthoflavivirus NS5-host protein-protein interactions. To this analysis, we used all the host factors identified in S2 – S4 Tables, and the g:GOSt application available at the g:Profiler website [102].

11. REFERENCES

1. Lim A, Shearer FM, Sewalk K, Pigott DM, Clarke J, Ghouse A, et al. The overlapping global distribution of dengue, chikungunya, Zika and yellow fever. Nat Commun. 2025;16: 3418. doi:10.1038/s41467-025-58609-5

2. Xu Y, Zhou J, Liu T, Liu P, Wu Y, Lai Z, et al. Assessing the risk of spread of Zika virus under current and future climate scenarios. Biosaf Health. 2022;4: 193–204. doi:10.1016/j.bsheal.2022.03.012

3. Malavige GN, Sjö P, Singh K, Piedagnel J-M, Mowbray C, Estani S, et al. Facing the escalating burden of dengue: Challenges and perspectives. PLOS Global Public Health. 2023;3: e0002598. doi:10.1371/journal.pgph.0002598

4. Pierson TC, Diamond MS. The continued threat of emerging flaviviruses. Nat Microbiol. 2020;5: 796–812. doi:10.1038/s41564-020-0714-0

5. de Souza WM, Weaver SC. Effects of climate change and human activities on vector-borne diseases. Nat Rev Microbiol. 2024;22: 476–491. doi:10.1038/s41579-024-01026-0

6. Roiz D, Pontifes PA, Jourdain F, Diagne C, Leroy B, Vaissière A-C, et al. The rising global economic costs of invasive Aedes mosquitoes and Aedes-borne diseases. Sci Total Environ. 2024;933: 173054. doi:10.1016/j.scitotenv.2024.173054

7. Moore SM, Oidtman RJ, James Soda K, Siraj AS, Reiner RC, Barker CM, et al. Leveraging multiple data types to estimate the size of the Zika epidemic in the Americas. PLoS Negl Trop Dis. 2020;14: e0008640. doi:10.1371/JOURNAL.PNTD.0008640

8. Cochet A, Calba C, Jourdain F, Grard G, Durand GA, Guinard A, et al. Autochthonous dengue in mainland France, 2022: geographical extension and incidence increase. Eurosurveillance. 2022;27: 1. doi:10.2807/1560-7917.ES.2022.27.44.2200818

9. Musso D, Ko AI, Baud D. Zika Virus Infection — After the Pandemic. New England Journal of Medicine. 2019;381: 1444–1457. doi:10.1056/nejmra1808246

10. Miner JJ, Diamond MS. Zika Virus Pathogenesis and Tissue Tropism. Cell Host Microbe. 2017;21: 134–142. doi:10.1016/j.chom.2017.01.004

11. Ferraris P, Yssel H, Missé D. Zika virus infection: an update. Microbes Infect. 2019;21: 353–360. doi:10.1016/j.micinf.2019.04.005

982 12. Santana LMB, de Moura IA, Mouzinho Ramos Tanaka Y, França RF de O. Zika Virus: A Review of
983 Biology, Clinical Impacts, and Coinfections. Viruses. 2025;17: 637. doi:10.3390/v17050637

984 13. Scaramozzino P, Carvelli A, Bruni G, Cappiello G, Censi F, Magliano A, et al. West Nile and Usutu
985 viruses co-circulation in central Italy: outcomes of the 2018 integrated surveillance. Parasit Vectors.
986 2021;14: 243. Available: https://parasitesandvectors.biomedcentral.com/articles/10.1186/s13071-
987 021-04736-z

988 14. Brüssow H, Figuerola J. The Spread of the Mosquito-Transmitted West Nile Virus in North America
989 and Europe. Microb Biotechnol. 2025;18. doi:10.1111/1751-7915.70120

990 15. Moir M, Sitharam N, Hofstra LM, Dor G, Mwanyika G, Ramphal Y, et al. Identifying genomic
991 surveillance gaps in Africa for the global public health response to West Nile virus: a systematic
992 review. Lancet Microbe. 2025;6: 101176. doi:10.1016/j.lanmic.2025.101176

993 16. Simonin Y. Un second cas autochtone d'infection par le virus Usutu détecté en France : que faut-il
994 savoir ? In: The Conversation [Internet]. 2022 [cited 16 Jan 2023]. Available:
995 https://theconversation.com/un-second-cas-autochtone-dinfection-par-le-virus-usutu-detecte-en-
996 france-que-faut-il-savoir-97944

997 17. Clé M, Beck C, Salinas S, Lecollinet S, Gutierrez S, Van de Perre P, et al. Usutu virus: A new threat?
998 Epidemiol Infect. 2019;147: e232. doi:10.1017/S0950268819001213

999 18. Simonin Y. Circulation of West Nile Virus and Usutu Virus in Europe: Overview and Challenges.
1000 Viruses. 2024;16: 599. doi:10.3390/v16040599

1001 19. Cadar D, Maier P, Müller S, Kress J, Chudy M, Bialonski A, et al. Blood donor screening for West Nile
1002 virus (WNV) revealed acute Usutu virus (USUV) infection, Germany, September 2016.
1003 Eurosurveillance. 2017;22: 30501. doi:10.2807/1560-7917.ES.2017.22.14.30501

1004 20. Bakonyi T, Jungbauer C, Aberle SW, Kolodziejek J, Dimmel K, Stiasny K, et al. Usutu virus infections
1005 among blood donors, Austria, July and August 2017 – Raising awareness for diagnostic challenges.
1006 Eurosurveillance. 2017;22. doi:10.2807/1560-7917.ES.2017.22.41.17-00644

1007 21. Madere FS, Andrade da Silva AV, Okeze E, Tilley E, Grinev A, Konduru K, et al. Flavivirus infections
1008 and diagnostic challenges for dengue, West Nile and Zika Viruses. npj Viruses. 2025;3: 36.
1009 doi:10.1038/s44298-025-00114-z

1010 22. Wahaab A, Mustafa BE, Hameed M, Stevenson NJ, Anwar MN, Liu K, et al. Potential Role of Flavivirus
1011 NS2B-NS3 Proteases in Viral Pathogenesis and Anti-flavivirus Drug Discovery Employing Animal Cells
1012 and Models: A Review. Viruses. 2021;14: 44. doi:10.3390/v14010044

1013 23. Ferrero DS, Ruiz-Arroyo VM, Soler N, Usón I, Guarné A, Verdaguer N. Supramolecular arrangement
1014 of the full-length Zika virus NS5. Rey FA, editor. PLoS Pathog. 2019;15: e1007656.
1015 doi:10.1371/journal.ppat.1007656

1016 24. Denolly S, Stukalov A, Barayeu U, Rosinski AN, Kritsiligkou P, Joecks S, et al. Zika virus remodelled ER
1017 membranes contain proviral factors involved in redox and methylation pathways. Nat Commun.
1018 2023;14: 8045. doi:10.1038/s41467-023-43665-6

1019 25. Welsch S, Miller S, Romero-Brey I, Merz A, Bleck CKE, Walther P, et al. Composition and three-
1020 dimensional architecture of the dengue virus replication and assembly sites. Cell Host Microbe.
1021 2009;5: 365–75. doi:10.1016/j.chom.2009.03.007

1022 26. Ci Y, Shi L. Compartmentalized replication organelle of flavivirus at the ER and the factors involved.
1023 Cellular and Molecular Life Sciences 2021 78:11. 2021;78: 4939–4954. doi:10.1007/S00018-021-
1024 03834-6

1025 27. Scaturro P, Stukalov A, Haas DA, Cortese M, Draganova K, Płaszczyca A, et al. An orthogonal
1026 proteomic survey uncovers novel Zika virus host factors. Nature. 2018;561: 253–257.
1027 doi:10.1038/s41586-018-0484-5

1028 28. Schneider WM, Hoffmann HH. Flavivirus-host interactions: an expanding network of proviral and
1029 antiviral factors. Curr Opin Virol. 2022;52: 71–77. doi:10.1016/J.COVIRO.2021.11.007

1030 29. Li P, Wu J, Liu S, Lu R, Jiang H, Wang N, et al. The RNA polymerase of cytoplasmically replicating Zika
1031 virus binds with chromatin DNA in nuclei and regulates host gene transcription. Proc Natl Acad Sci U
1032 S A. 2022;119: e2205013119. doi:10.1073/pnas.2205013119

1033 30. Lebeau G, Hoareau M, Rivière S, El Safadi D, Da Silva CR, Krejbich-Trotot P, et al. Cell cycle and
1034 mitosis progression during ZIKA virus infection: The viral non-structural protein NS5 as a master
1035 regulator of the APC/cyclosome? Biochimie. 2024;221: 75–80. doi:10.1016/j.biochi.2024.01.016

1036 31. Best SM. The Many Faces of the Flavivirus NS5 Protein in Antagonism of Type I Interferon Signaling. J
1037 Virol. 2017;91. doi:10.1128/JVI.01970-16

1038 32. Albentosa-González L, Jimenez de Oya N, Arias A, Clemente-Casares P, Martin-Acebes MÁ, Saiz JC, et
1039 al. Akt Kinase Intervenes in Flavivirus Replication by Interacting with Viral Protein NS5. Viruses.
1040 2021;13: 896. Available: http://www.ncbi.nlm.nih.gov/pubmed/34066055

1041 33. Rodrigo I, Albentosa-González L, Romero de Ávila MJ, Bassi MR, Sempere RN, Clemente-Casares P,
1042 et al. Ubiquitin-like modifier-activating enzyme 1 interacts with Zika virus NS5 and promotes viral
1043 replication in the infected cell. J Gen Virol. 2025;106: 002063. doi:10.1099/jgv.0.002063

1044 34. Saade M, Ferrero DS, Blanco-Ameijeiras J, Gonzalez-Gobartt E, Flores-Mendez M, Ruiz-Arroyo VM, et
1045 al. Multimerization of Zika Virus-NS5 Causes Ciliopathy and Forces Premature Neurogenesis. Cell
1046 Stem Cell. 2020;27: 920-936.e8. doi:10.1016/j.stem.2020.10.002

1047 35. Deb A, Nagpal S, Yadav RK, Thakur H, Nair D, Krishnan V, et al. Japanese encephalitis virus NS5
1048 protein interacts with nucleolin to enhance the virus replication. J Virol. 2024;98: e0085824.
1049 doi:10.1128/jvi.00858-24

1050 36. Grant A, Ponia SS, Tripathi S, Balasubramaniam V, Miorin L, Sourisseau M, et al. Zika Virus Targets
1051 Human STAT2 to Inhibit Type i Interferon Signaling. Cell Host Microbe. 2016;19: 882–890.
1052 doi:10.1016/j.chom.2016.05.009

1053 37. Gonzalez Lopez Ledesma MM, Costa Navarro G, Pallares HM, Paletta A, De Maio F, Iglesias NG, et al.
1054 Dengue virus NS5 degrades ERC1 during infection to antagonize NF-kB activation. Proceedings of the
1055 National Academy of Sciences. 2023;120. doi:10.1073/pnas.2220005120

1056 38. Ren W, Fu C, Zhang Y, Ju X, Jiang X, Song J, et al. Zika virus NS5 protein inhibits type I interferon
1057 signaling via CRL3 E3 ubiquitin ligase-mediated degradation of STAT2. Proc Natl Acad Sci U S A.
1058 2024;121: e2403235121. doi:10.1073/pnas.2403235121

1059 39. Liu Y, Zhou T, Hu J, Jin S, Wu J, Guan X, et al. Targeting Selective Autophagy as a Therapeutic
1060 Strategy for Viral Infectious Diseases. Front Microbiol. 2022;13. doi:10.3389/fmicb.2022.889835

1061 40. Yan C, Gong L, Chen L, Xu M, Abou-Hamdan H, Tang M, et al. PHB2 (prohibitin 2) promotes PINK1-
1062 PRKN/Parkin-dependent mitophagy by the PARL-PGAM5-PINK1 axis. Autophagy. 2020;16: 419–434.
1063 doi:10.1080/15548627.2019.1628520

1064 41. Jin SM, Youle RJ. PINK1- and Parkin-mediated mitophagy at a glance. J Cell Sci. 2012;125: 795–799.
1065 doi:10.1242/jcs.093849

1066 42. Dagda RK, Cherra SJ, Kulich SM, Tandon A, Park D, Chu CT. Loss of PINK1 Function Promotes
1067 Mitophagy through Effects on Oxidative Stress and Mitochondrial Fission. Journal of Biological
1068 Chemistry. 2009;284: 13843–13855. doi:10.1074/jbc.M808515200

1069 43. Cheng M, Lin N, Dong D, Ma J, Su J, Sun L. PGAM5: A crucial role in mitochondrial dynamics and
1070 programmed cell death. Eur J Cell Biol. 2021;100: 151144. Available:
1071 https://linkinghub.elsevier.com/retrieve/pii/S0171933520300832

1072 44. Xiao Y, Zhou Y, Lu Y, Zhou K, Cai W. PHB2 interacts with LC3 and SQSTM1 is required for bile acids-
1073 induced mitophagy in cholestatic liver. Cell Death Dis. 2018;9: 160. doi:10.1038/s41419-017-0228-8

1074 45. Boytz R, Keita K, Pawlak JB, Laurent-Rolle M. Flaviviruses manipulate mitochondrial processes to
1075 evade the innate immune response. npj Viruses. 2024;2: 47. doi:10.1038/s44298-024-00057-x

1076 46. Agarwal A, Alam MF, Basu B, Pattanayak S, Asthana S, Syed GH, et al. Japanese Encephalitis Virus
1077 NS4A Protein Interacts with PTEN-Induced Kinase 1 (PINK1) and Promotes Mitophagy in Infected
1078 Cells. Ramage H, editor. Microbiol Spectr. 2022;10: e0083022. Available:
1079 http://www.ncbi.nlm.nih.gov/pubmed/35604158

1080 47. Khan M, Syed GH, Kim SJ, Siddiqui A. Mitochondrial dynamics and viral infections: A close nexus.
1081 Biochim Biophys Acta. 2015;1853: 2822–2833. doi:10.1016/J.BBAMCR.2014.12.040

1082 48. Singh B, Avula K, Sufi SA, Parwin N, Das S, Alam MF, et al. Defective Mitochondrial Quality Control
1083 during Dengue Infection Contributes to Disease Pathogenesis. Ou J-HJ, editor. J Virol. 2022;96:
1084 e0082822. Available: http://www.ncbi.nlm.nih.gov/pubmed/36197108

1085 49. Ponia SS, Robertson SJ, McNally KL, Subramanian G, Sturdevant GL, Lewis M, et al. Mitophagy
1086 antagonism by ZIKV reveals Ajuba as a regulator of PINK1 signaling, PKR-dependent inflammation,
1087 and viral invasion of tissues. Cell Rep. 2021;37: 109888. Available:
1088 https://linkinghub.elsevier.com/retrieve/pii/S2211124721013589

1089 50. Lee JK, Shin OS. Zika virus modulates mitochondrial dynamics, mitophagy, and mitochondria-derived
1090 vesicles to facilitate viral replication in trophoblast cells. Front Immunol. 2023;14.
1091 doi:10.3389/fimmu.2023.1203645

1092 51. Bassi MR, Sempere RN, Meyn P, Polacek C, Arias A. Extinction of Zika virus and Usutu virus by lethal
1093 mutagenesis reveals different patterns of sensitivity to three mutagenic drugs. Antimicrob Agents
1094 Chemother. 2018;62: e00380-18. doi:10.1128/AAC.00380-18

1095 52. Sempere RN, Arias A. Establishment of a Cell Culture Model of Persistent Flaviviral Infection: Usutu
1096 Virus Shows Sustained Replication during Passages and Resistance to Extinction by Antiviral
1097 Nucleosides. Viruses. 2019;11: 560. Available: https://www.mdpi.com/1999-4915/11/6/560

1098 53. Martínez-González B, Gallego I, Gregori J, Soria ME, Somovilla P, de Ávila AI, et al. Fitness-
1099 Dependent, Mild Mutagenic Activity of Sofosbuvir for Hepatitis C Virus. Antimicrob Agents
1100 Chemother. 2023;67. doi:10.1128/aac.00394-23

1101 54. Rodrigo I, Ballesta C, Nunes EB, Pérez P, García-Arriaza J, Arias A. Eeyarestatin I, an inhibitor of the
1102 valosin-containing protein, exhibits potent virucidal activity against the flaviviruses. Antiviral Res.
1103 2022;207: 105416. doi:10.1016/J.ANTIVIRAL.2022.105416

1104 55. Lindenbach BD. Measuring HCV Infectivity Produced in Cell Culture and In Vivo. Methods in
1105 molecular biology (Clifton, NJ). 2009. pp. 329–336. doi:10.1007/978-1-59745-394-3_24

1106 56. Reed LJ, Muench H. A simple method of estimating fifty per cent endpoints. Am J Epidemiol.
1107 1938;27: 493–497. doi:10.1093/oxfordjournals.aje.a118408

1108 57. Livak KJ, Schmittgen TD. Analysis of relative gene expression data using real-time quantitative PCR
1109 and the 2-ΔΔCT method. Methods. 2001;25: 402–408. doi:10.1006/meth.2001.1262

1110 58. Albentosa-González L, Sabariegos R, Arias A, Clemente-Casares P, Mas A. Akt interacts with usutu
1111 virus polymerase, and its activity modulates viral replication. Pathogens. 2021;10: 1–15.

1112 59. Hughes CS, Moggridge S, Müller T, Sorensen PH, Morin GB, Krijgsveld J. Single-pot, solid-phase-
1113 enhanced sample preparation for proteomics experiments. Nat Protoc. 2019;14: 68–85.
1114 doi:10.1038/s41596-018-0082-x

1115 60. Meyer B, Chiaravalli J, Gellenoncourt S, Brownridge P, Bryne DP, Daly LA, et al. Characterising
1116 proteolysis during SARS-CoV-2 infection identifies viral cleavage sites and cellular targets with
1117 therapeutic potential. Nature Communications 2021 12:1. 2021;12: 1–16. doi:10.1038/s41467-021-
1118 25796-w

1119 61. Cox J, Mann M. MaxQuant enables high peptide identification rates, individualized p.p.b.-range
1120 mass accuracies and proteome-wide protein quantification. Nat Biotechnol. 2008;26: 1367–1372.
1121 doi:10.1038/nbt.1511

1122 62. Nguyen SK, Anders N, Holmes S, Barrow HG, Lukhovitskaya N, Jahun AS, et al. Encephalomyocarditis
1123 virus protein 2B* interacts with 14-3-3 proteins through a phosphorylated C-terminal binding motif.
1124 mBio. 2025;16. doi:10.1128/mbio.01008-25

1125 63. Zhang T, Li J, He Y, Yang F, Hao Y, Jin W, et al. A small molecule targeting myoferlin exerts promising
1126 anti-tumor effects on breast cancer. Nat Commun. 2018;9: 3726. doi:10.1038/s41467-018-06179-0

1127 64. Bordt EA, Clerc P, Roelofs BA, Saladino AJ, Tretter L, Adam-Vizi V, et al. The Putative Drp1 Inhibitor
1128 mdivi-1 Is a Reversible Mitochondrial Complex I Inhibitor that Modulates Reactive Oxygen Species.
1129 Dev Cell. 2017;40: 583-594.e6. doi:10.1016/j.devcel.2017.02.020

1130 65. Yoshinaka T, Kosako H, Yoshizumi T, Furukawa R, Hirano Y, Kuge O, et al. Structural Basis of
1131 Mitochondrial Scaffolds by Prohibitin Complexes: Insight into a Role of the Coiled-Coil Region.
1132 iScience. 2019;19: 1065. doi:10.1016/J.ISCI.2019.08.056

1133 66. Zhou P, Zhang Q, Yang Y, Wu W, Chen D, Zheng Z, et al. Cleavage of SQSTM1/p62 by the Zika virus
1134 protease NS2B3 prevents autophagic degradation of viral NS3 and NS5 proteins. Autophagy.
1135 2024;20: 2769–2784. doi:10.1080/15548627.2024.2390810

1136 67. Ding Q, Gaska JM, Douam F, Wei L, Kim D, Balev M, et al. Species-specific disruption of STING-
1137 dependent antiviral cellular defenses by the Zika virus NS2B3 protease. Proceedings of the National
1138 Academy of Sciences. 2018;115. doi:10.1073/pnas.1803406115

1139 68. Lennemann NJ, Coyne CB. Dengue and Zika viruses subvert reticulophagy by NS2B3-mediated
1140 cleavage of FAM134B. Autophagy. 2017;13: 322–332. doi:10.1080/15548627.2016.1265192

1141 69. Wang L, Zhang X, Huang X, Sha X, Li X, Zheng J, et al. Homoplantaginin alleviates high
1142 glucose-induced vascular endothelial senescence by inhibiting mtDNA–cGAS–STING pathway via
1143 blunting DRP1–mitochondrial fission–VDAC1 axis. The FASEB Journal. 2024;38.
1144 doi:10.1096/fj.202401299RR

1145 70. Qi Y, Rajbanshi B, Hao R, Dang Y, Xu C, Lu W, et al. The dual role of PGAM5 in inflammation. Exp Mol
1146 Med. 2025;57: 298–311. doi:10.1038/s12276-025-01391-7

1147 71. Bavelloni A, Piazzi M, Raffini M, Faenza I, Blalock WL. Prohibitin 2: At a communications crossroads.
1148 IUBMB Life. 2015;67: 239–254. doi:10.1002/iub.1366

1149 72. Sun L, Liu L, Yang X-J, Wu Z. Akt binds prohibitin 2 and relieves its repression of MyoD and muscle
1150 differentiation. J Cell Sci. 2004;117: 3021–3029. doi:10.1242/jcs.01142

1151 73. Ding T, Xu H, Zhang X, Yang F, Zhang J, Shi Y, et al. Prohibitin 2 orchestrates long noncoding RNA and
1152 gene transcription to accelerate tumorigenesis. Nat Commun. 2024;15: 8385. doi:10.1038/s41467-
1153 024-52425-z

1154 74. Kasashima K, Ohta E, Kagawa Y, Endo H. Mitochondrial Functions and Estrogen Receptor-dependent
1155 Nuclear Translocation of Pleiotropic Human Prohibitin 2. Journal of Biological Chemistry. 2006;281:
1156 36401–36410. doi:10.1074/jbc.M605260200

1157 75. Kim J, Akiyama M, Park J, Lin M, Shimo A, Ueki T, et al. Activation of an estrogen/estrogen receptor
1158 signaling by BIG3 through its inhibitory effect on nuclear transport of PHB2/REA in breast cancer.
1159 Cancer Sci. 2009;100: 1468–1478. doi:10.1111/j.1349-7006.2009.01209.x

1160 76. Grady SF, Pinto AK, Hassert M, D'Angelo JA, Brien JD, Arnatt CK. Selective estrogen receptor
1161 modulator, tamoxifen, inhibits Zika virus infection. J Med Virol. 2021;93: 6155–6162.
1162 doi:10.1002/JMV.27230

1163 77. Oyang L, Li J, Jiang X, Lin J, Xia L, Yang L, et al. The function of prohibitins in mitochondria and the
1164 clinical potentials. Cancer Cell Int. 2022;22: 343. Available:
1165 https://cancerci.biomedcentral.com/articles/10.1186/s12935-022-02765-x

1166 78. Eyre NS, Kirby EN, Anfiteatro DR, Bracho G, Russo AG, White PA, et al. Identification of Estrogen
1167 Receptor Modulators as Inhibitors of Flavivirus Infection. Antimicrob Agents Chemother. 2020;64:
1168 e00289-20. Available: https://journals.asm.org/doi/10.1128/AAC.00289-20

1169 79. Celegato M, Sturlese M, Vasconcelos Costa V, Trevisan M, Lallo Dias AS, Souza Passos IB, et al. Small-
1170 Molecule Inhibitor of Flaviviral NS3-NS5 Interaction with Broad-Spectrum Activity and Efficacy *In*
1171 *Vivo*. mBio. 2023;14. doi:10.1128/mbio.03097-22

1172 80. Tay MYF, Saw WG, Zhao Y, Chan KWK, Singh D, Chong Y, et al. The C-terminal 50 Amino Acid
1173 Residues of Dengue NS3 Protein Are Important for NS3-NS5 Interaction and Viral Replication.
1174 Journal of Biological Chemistry. 2015;290: 2379–2394. doi:10.1074/jbc.M114.607341

1175 81. Zoladek J, Nisole S. Mosquito-borne flaviviruses and type I interferon: catch me if you can! Front
1176 Microbiol. 2023;14. doi:10.3389/fmicb.2023.1257024

1177 82. Goh JZH, De Hayr L, Khromykh AA, Slonchak A. The Flavivirus Non-Structural Protein 5 (NS5):
1178 Structure, Functions, and Targeting for Development of Vaccines and Therapeutics. Vaccines (Basel).
1179 2024;12: 865. doi:10.3390/vaccines12080865

1180 83. Rehwinkel J, Gack MU. RIG-I-like receptors: their regulation and roles in RNA sensing. Nat Rev
1181 Immunol. 2020;20: 537–551. doi:10.1038/S41577-020-0288-3

1182 84. Pan Y, Cai W, Cheng A, Wang M, Yin Z, Jia R. Flaviviruses: Innate Immunity, Inflammasome
1183 Activation, Inflammatory Cell Death, and Cytokines. Front Immunol. 2022;13: 829433.
1184 doi:10.3389/fimmu.2022.829433

1185 85. Jiménez-Loygorri JI, Villarejo-Zori B, Viedma-Poyatos Á, Zapata-Muñoz J, Benítez-Fernández R,
1186 Frutos-Lisón MD, et al. Mitophagy curtails cytosolic mtDNA-dependent activation of cGAS/STING
1187 inflammation during aging. Nat Commun. 2024;15: 830. doi:10.1038/s41467-024-45044-1

1188 86. Yuk J-M, Silwal P, Jo E-K. Inflammasome and Mitophagy Connection in Health and Disease. Int J Mol
1189 Sci. 2020;21: 4714. doi:10.3390/ijms21134714

1190 87. Fu C, Cao N, Liu W, Zhang Z, Yang Z, Zhu W, et al. Crosstalk between mitophagy and innate immunity
1191 in viral infection. Front Microbiol. 2022;13. doi:10.3389/fmicb.2022.1064045

1192 88. Wang S, Long H, Hou L, Feng B, Ma Z, Wu Y, et al. The mitophagy pathway and its implications in
1193 human diseases. Signal Transduct Target Ther. 2023;8: 304. doi:10.1038/s41392-023-01503-7

1194 89. Gkikas I, Palikaras K, Tavernarakis N. The Role of Mitophagy in Innate Immunity. Front Immunol.
1195 2018;9: 1283. doi:10.3389/FIMMU.2018.01283

1196 90. Jin Y, Zhao L, Wang S, Zhang X, Quan J, Lin Z, et al. *RSL1D1* knockdown induces ferroptosis and
1197 mediates ferrous iron accumulation in senescent cells by inhibiting *FTH1* mRNA stability.
1198 Carcinogenesis. 2023;44: 129–142. doi:10.1093/carcin/bgad012

1199 91. Liu X, Chen J, Long X, Lan J, Liu X, Zhou M, et al. RSL1D1 promotes the progression of colorectal
1200 cancer through RAN-mediated autophagy suppression. Cell Death Dis. 2022;13: 43.
1201 doi:10.1038/s41419-021-04492-z

1202 92. Gupta S, Yano J, Mercier V, Htwe HH, Shin HR, Rademaker G, et al. Lysosomal retargeting of
1203 Myoferlin mitigates membrane stress to enable pancreatic cancer growth. Nat Cell Biol. 2021;23:
1204 232–242. doi:10.1038/s41556-021-00644-7

1205 93. Bernatchez PN, Sharma A, Kodaman P, Sessa WC. Myoferlin is critical for endocytosis in endothelial
1206 cells. American Journal of Physiology-Cell Physiology. 2009;297: C484–C492.
1207 doi:10.1152/ajpcell.00498.2008

1208 94. Morita E, Suzuki Y. Membrane-Associated Flavivirus Replication Complex—Its Organization and
1209 Regulation. Viruses. 2021;13: 1060. doi:10.3390/v13061060

1210 95. Cretu C, Chernev A, Kibédi Szabó CZ, Pena V, Urlaub H, Moser T, et al. Structural insights into lipid
1211 membrane binding by human ferlins. EMBO J. 2025. doi:10.1038/s44318-025-00463-8

1212 96. He Y, Kan W, Li Y, Hao Y, Huang A, Gu H, et al. A potent and selective small molecule inhibitor of
1213 myoferlin attenuates colorectal cancer progression. Clin Transl Med. 2021;11. doi:10.1002/ctm2.289

1214 97. Xu G, Xia Z, Deng F, Liu L, Wang Q, Yu Y, et al. Inducible LGALS3BP/90K activates antiviral innate
1215 immune responses by targeting TRAF6 and TRAF3 complex. PLoS Pathog. 2019;15: e1008002.
1216 doi:10.1371/journal.ppat.1008002

1217 98. Arutyunov A, Durán-Laforet V, Ai S, Ferrari L, Murphy R, Schafer DP, et al. West Nile Virus-Induced
1218 Expression of Senescent Gene Lgals3bp Regulates Microglial Phenotype within Cerebral Cortex.
1219 Biomolecules. 2024;14: 808. doi:10.3390/biom14070808

1220 99. Hulsen T, de Vlieg J, Alkema W. BioVenn – a web application for the comparison and visualization of
1221 biological lists using area-proportional Venn diagrams. BMC Genomics. 2008;9: 488.
1222 doi:10.1186/1471-2164-9-488

1223 100. Szklarczyk D, Kirsch R, Koutrouli M, Nastou K, Mehryary F, Hachilif R, et al. The STRING database in
1224 2023: protein–protein association networks and functional enrichment analyses for any sequenced
1225 genome of interest. Nucleic Acids Res. 2023;51: D638–D646. doi:10.1093/nar/gkac1000

1226 101. Shannon P, Markiel A, Ozier O, Baliga NS, Wang JT, Ramage D, et al. Cytoscape: A Software
1227 Environment for Integrated Models of Biomolecular Interaction Networks. Genome Res. 2003;13:
1228 2498–2504. doi:10.1101/gr.1239303

1229 102. Kolberg L, Raudvere U, Kuzmin I, Adler P, Vilo J, Peterson H. g:Profiler—interoperable web service
1230 for functional enrichment analysis and gene identifier mapping (2023 update). Nucleic Acids Res.
1231 2023;51: W207–W212. doi:10.1093/nar/gkad347

1232

1233

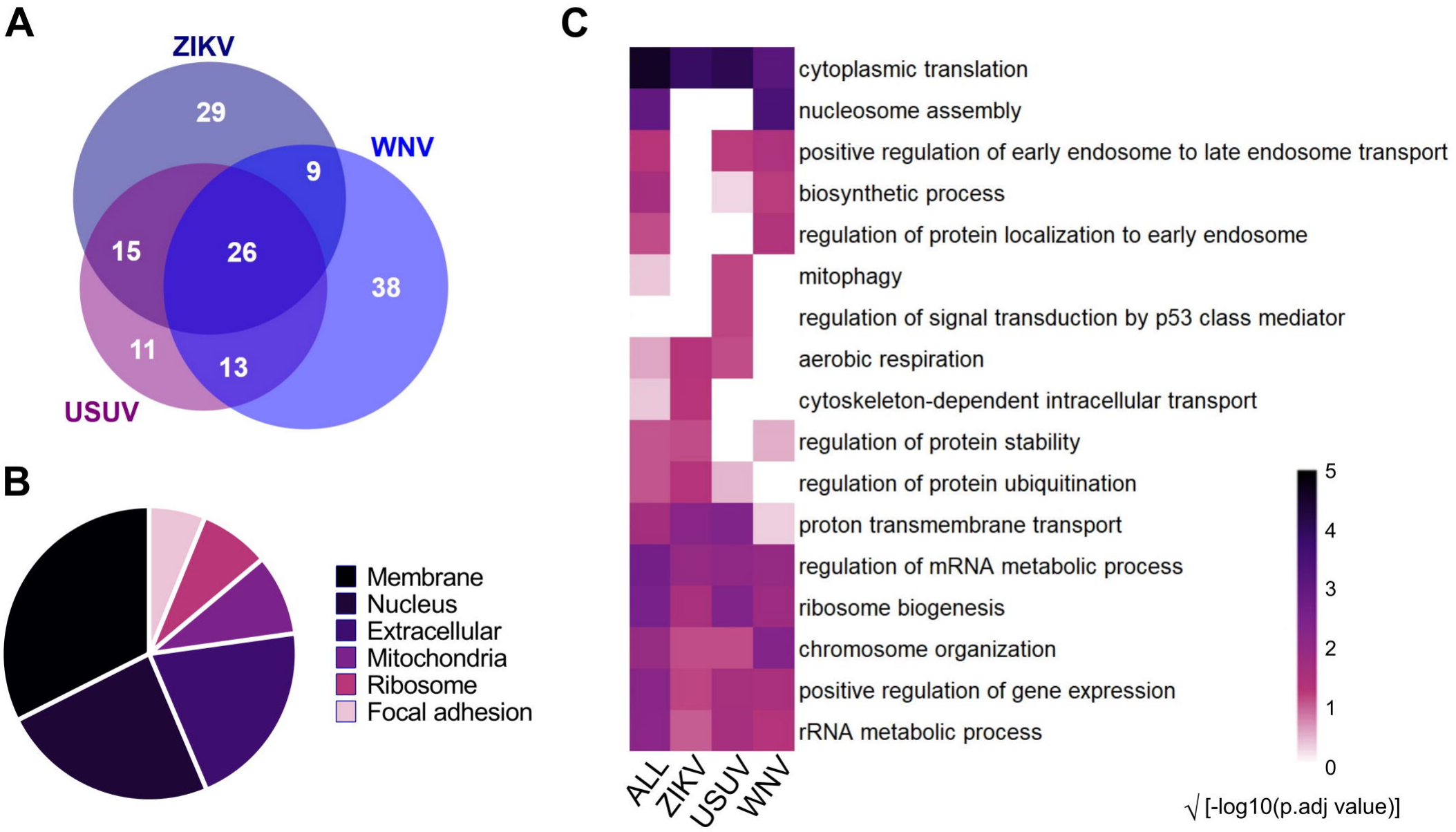
A
ZIKV
WNV
USUV
29
9
15
26
38
11
13
B
Membrane
Nucleus
Extracellular
Mitochondria
Ribosome
Focal adhesion
C
cytoplasmic translation
nucleosome assembly
positive regulation of early endosome to late endosome transport
biosynthetic process
regulation of protein localization to early endosome
mitophagy
regulation of signal transduction by p53 class mediator
aerobic respiration
cytoskeleton-dependent intracellular transport
regulation of protein stability
regulation of protein ubiquitination
proton transmembrane transport
regulation of mRNA metabolic process
ribosome biogenesis
chromosome organization
positive regulation of gene expression
rRNA metabolic process
ALL
ZIKV
USUV
WNV
5
4
3
2
1
0
√ [-log10(p.adj value)]

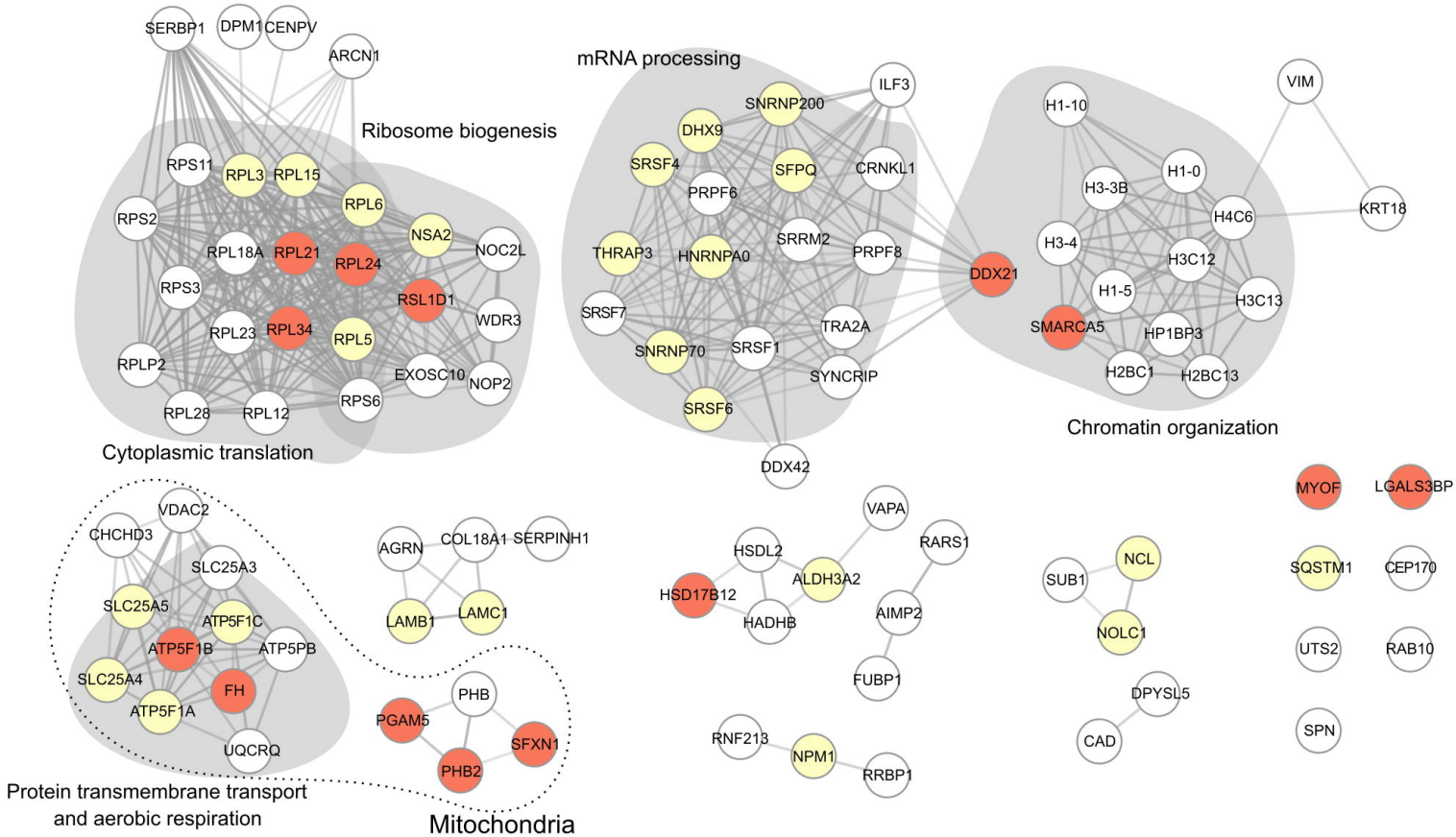
SERBP1
DPM1
CENPV
ARCN1
Ribosome biogenesis
RPS11
RPL3
RPL15
RPL6
RPS2
NSA2
NOC2L
RPL18A
RPL21
RPL24
RPS3
RSL1D1
WDR3
RPL23
RPL34
RPL5
RPLP2
EXOSC10
NOP2
RPS6
RPL28
RPL12
Cytoplasmic translation
mRNA processing
ILF3
SNRNP200
DHX9
SRSF4
SFPQ
CRNKL1
PRPF6
SRRM2
THRAP3
HNRNPA0
PRPF8
SRSF7
TRA2A
SNRNP70
SRSF1
SYNCRIP
SRSF6
DDX42
DDX21
VIM
H1-10
H1-0
H3-3B
H4C6
KRT18
H3-4
H3C12
H1-5
H3C13
SMARCA5
HP1BP3
H2BC1
H2BC13
Chromatin organization
VDAC2
CHCHD3
SLC25A3
SLC25A5
ATP5F1C
ATP5F1B
ATP5PB
SLC25A4
FH
ATP5F1A
UQCRQ
Protein transmembrane transport
and aerobic respiration
AGRN
COL18A1
SERPINH1
LAMB1
LAMC1
PHB
PGAM5
SFXN1
PHB2
Mitochondria
VAPA
HSDL2
RARS1
ALDH3A2
HSD17B12
AIMP2
HADHB
FUBP1
RNF213
NPM1
RRBP1
SUB1
NCL
NOLC1
DPYSL5
CAD
MYOF
LGALS3BP
SQSTM1
CEP170
UTS2
RAB10
SPN

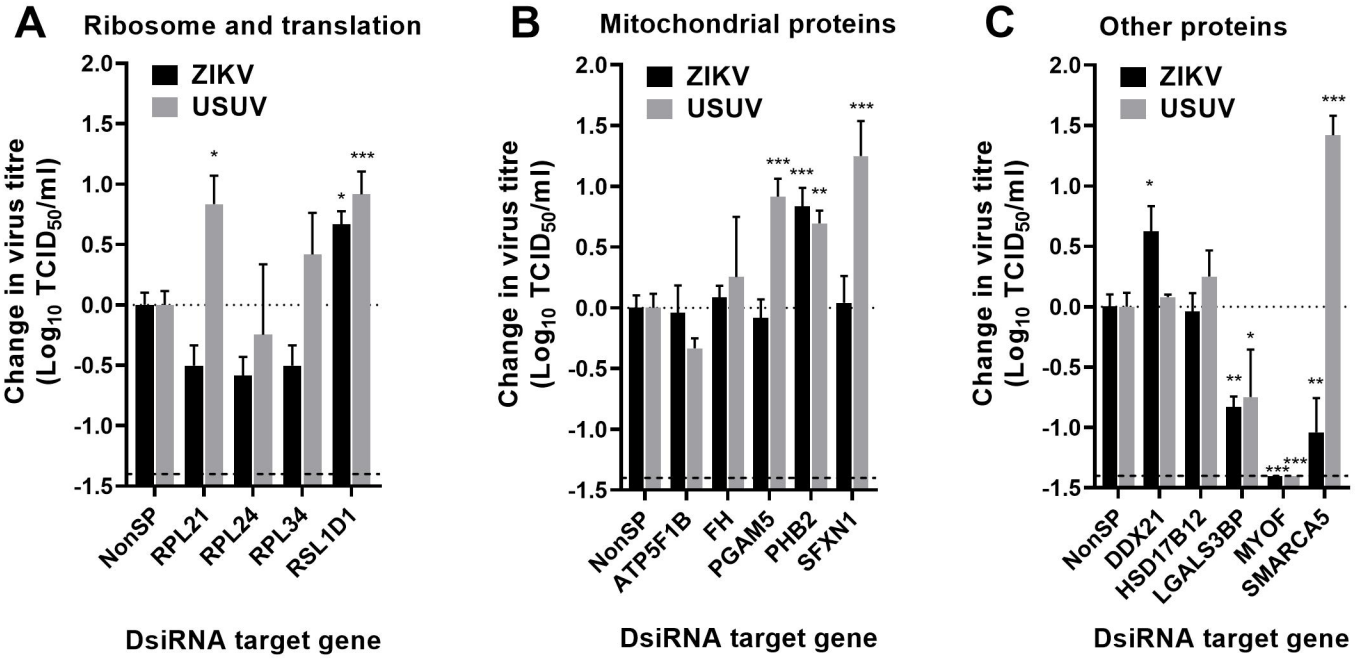
A
Ribosome and translation
ZIKV
USUV
Change in virus titre
(Log10 TCID50/ml)
2.0
1.5
1.0
0.5
0.0
-0.5
-1.0
-1.5
*
*
***
NonSP
RPL21
RPL24
RPL34
RSL1D1
DsiRNA target gene
B
Mitochondrial proteins
ZIKV
USUV
Change in virus titre
(Log10 TCID50/ml)
***
***
**
***
NonSP
ATP5F1B
FH
PGAM5
PHB2
SFXN1
DsiRNA target gene
C
Other proteins
ZIKV
USUV
Change in virus titre
(Log10 TCID50/ml)
*
**
*
**
***
***
***
NonSP
DDX21
HSD17B12
LGALS3BP
MYOF
SMARCA5
DsiRNA target gene

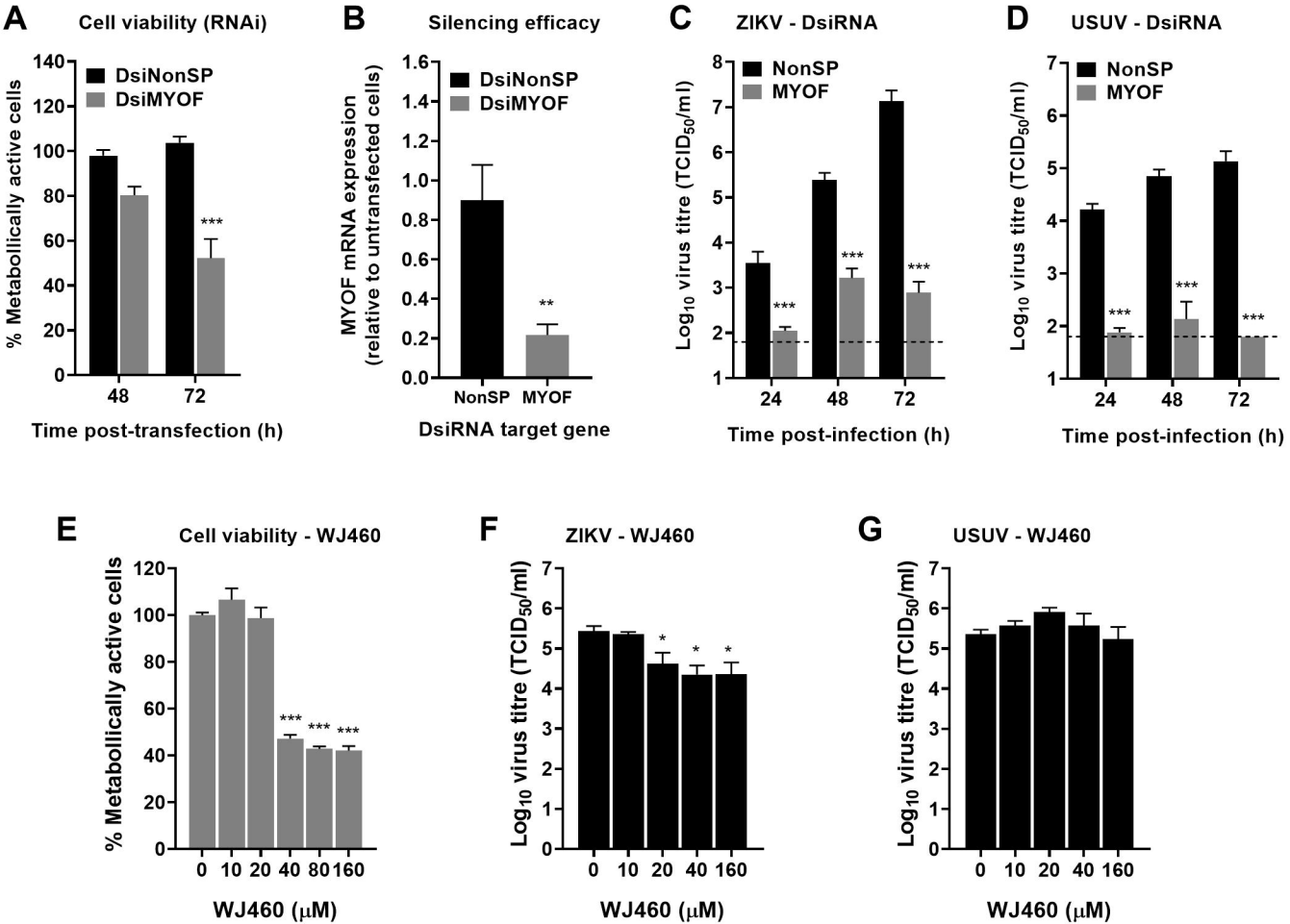
A
Cell viability (RNAi)
DsiNonSP
DsiMYOF
% Metabollically active cells
140
120
100
80
60
40
20
0
***
48
72
Time post-transfection (h)
B
Silencing efficacy
DsiNonSP
DsiMYOF
MYOF mRNA expression (relative to untransfected cells)
1.6
1.4
1.2
1.0
0.8
0.6
0.4
0.2
0.0
**
NonSP
MYOF
DsiRNA target gene
C
ZIKV - DsiRNA
NonSP
MYOF
Log10 virus titre (TCID50/ml)
8
7
6
5
4
3
2
1
***
24
48
72
Time post-infection (h)
D
USUV - DsiRNA
NonSP
MYOF
Log10 virus titre (TCID50/ml)
7
6
5
4
3
2
1
***
24
48
72
Time post-infection (h)
E
Cell viability - WJ460
% Metabollically active cells
120
100
80
60
40
20
0
***
***
***
0
10
20
40
80
160
WJ460 (μM)
F
ZIKV - WJ460
Log10 virus titre (TCID50/ml)
7
6
5
4
3
2
1
0
*
*
*
0
10
20
40
160
WJ460 (μM)
G
USUV - WJ460
Log10 virus titre (TCID50/ml)
7
6
5
4
3
2
1
0
0
10
20
40
160
WJ460 (μM)

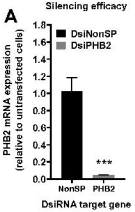
A
Silencing efficacy
DsiNonSP
DsiPHB2
PHB2 mRNA expression (relative to untransfected cells)
1.8
1.6
1.4
1.2
1.0
0.8
0.6
0.4
0.2
0.0
***
NonSP
PHB2
DsiRNA target gene

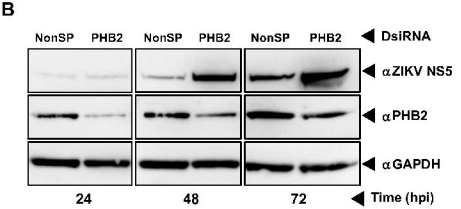
B
NonSP
PHB2
NonSP
PHB2
NonSP
PHB2
DsiRNA
αZIKV NS5
αPHB2
αGAPDH
24
48
72
Time (hpi)

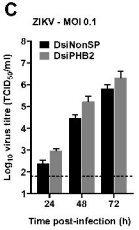
C
ZIKV - MOI 0.1
DsiNonSP
DsiPHB2
Log10 virus titre (TCID50/ml)
Time post-infection (h)
24
48
72

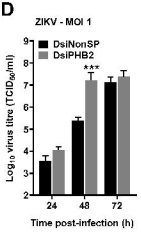
D
ZIKV - MOI 1
DsiNonSP
DsiPHB2
***
Log10 virus titre (TCID50/ml)
Time post-infection (h)
24
48
72

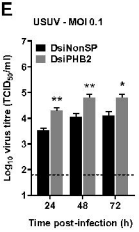
E
USUV - MOI 0.1
DsiNonSP
DsiPHB2
**
**
*
Log10 virus titre (TCID50/ml)
Time post-infection (h)
24
48
72

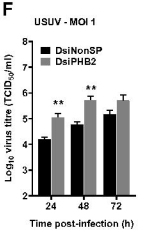
F
USUV - MOI 1
DsiNonSP
DsiPHB2
**
**
Log10 virus titre (TCID50/ml)
Time post-infection (h)
24
48
72

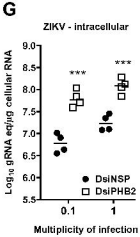
G
ZIKV - intracellular
***
***
Log10 gRNA eq/µg cellular RNA
DsiNSP
DsiPHB2
0.1
1
Multiplicity of infection

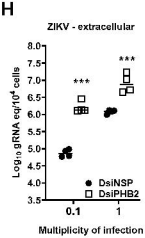
H
ZIKV - extracellular
***
***
Log10 gRNA eq/10^4 cells
DsiNSP
DsiPHB2
0.1
1
Multiplicity of infection

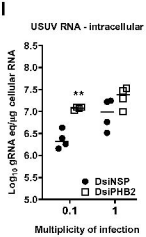
I
USUV RNA - intracellular
**
Log10 gRNA eq/µg cellular RNA
DsiNSP
DsiPHB2
0.1
1
Multiplicity of infection

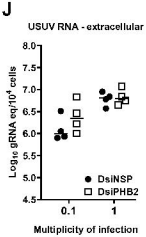
J
USUV RNA - extracellular
Log10 gRNA eq/10^4 cells
DsiNSP
DsiPHB2
0.1
1
Multiplicity of infection

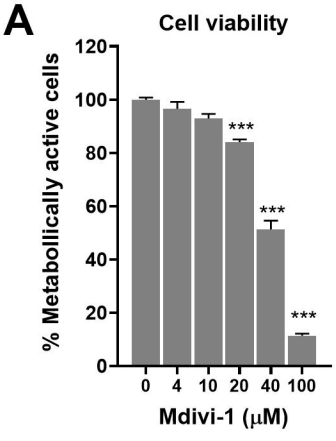
A
Cell viability
% Metabollically active cells
120
100
80
60
40
20
0
***
***
***
0
4
10
20
40
100
Mdivi-1 (μM)

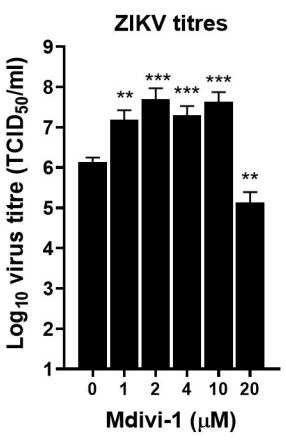
B
ZIKV titres
Log10 virus titre (TCID50/ml)
9
8
7
6
5
4
3
2
1
**
***
***
***
**
0
1
2
4
10
20
Mdivi-1 (μM)

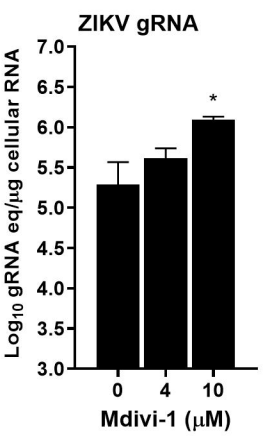
C
ZIKV gRNA
Log10 gRNA eq/μg cellular RNA
7.0
6.5
6.0
5.5
5.0
4.5
4.0
3.5
3.0
*
0
4
10
Mdivi-1 (μM)

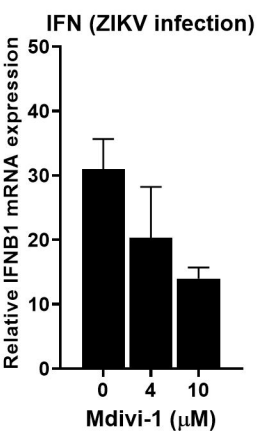
D
IFN (ZIKV infection)
Relative IFNB1 mRNA expression
50
40
30
20
10
0
0
4
10
Mdivi-1 (μM)

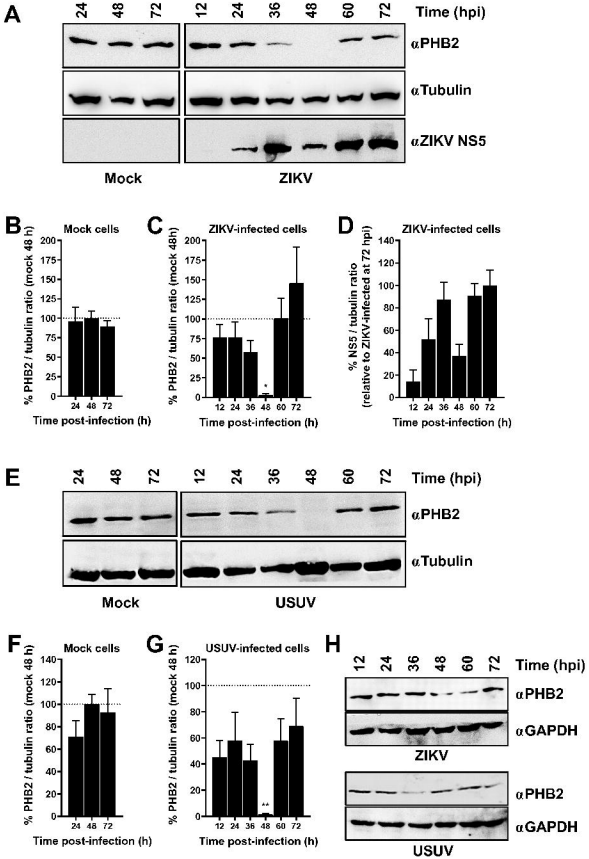
A
24
48
72
12
24
36
48
60
72
Time (hpi)
αPHB2
αTubulin
αZIKV NS5
Mock
ZIKV
B
Mock cells
% PHB2 / tubulin ratio (mock 48 h)
Time post-infection (h)
C
ZIKV-infected cells
% PHB2 / tubulin ratio (mock 48h)
Time post-infection (h)
D
ZIKV-infected cells
% NS5 / tubulin ratio
(relative to ZIKV-infected at 72 hpi)
Time post-infection (h)
E
Time (hpi)
αPHB2
αTubulin
Mock
USUV
F
Mock cells
% PHB2 / tubulin ratio (mock 48 h)
Time post-infection (h)
G
USUV-infected cells
% PHB2 / tubulin ratio (mock 48 h)
Time post-infection (h)
H
Time (hpi)
αPHB2
αGAPDH
ZIKV
αPHB2
αGAPDH
USUV

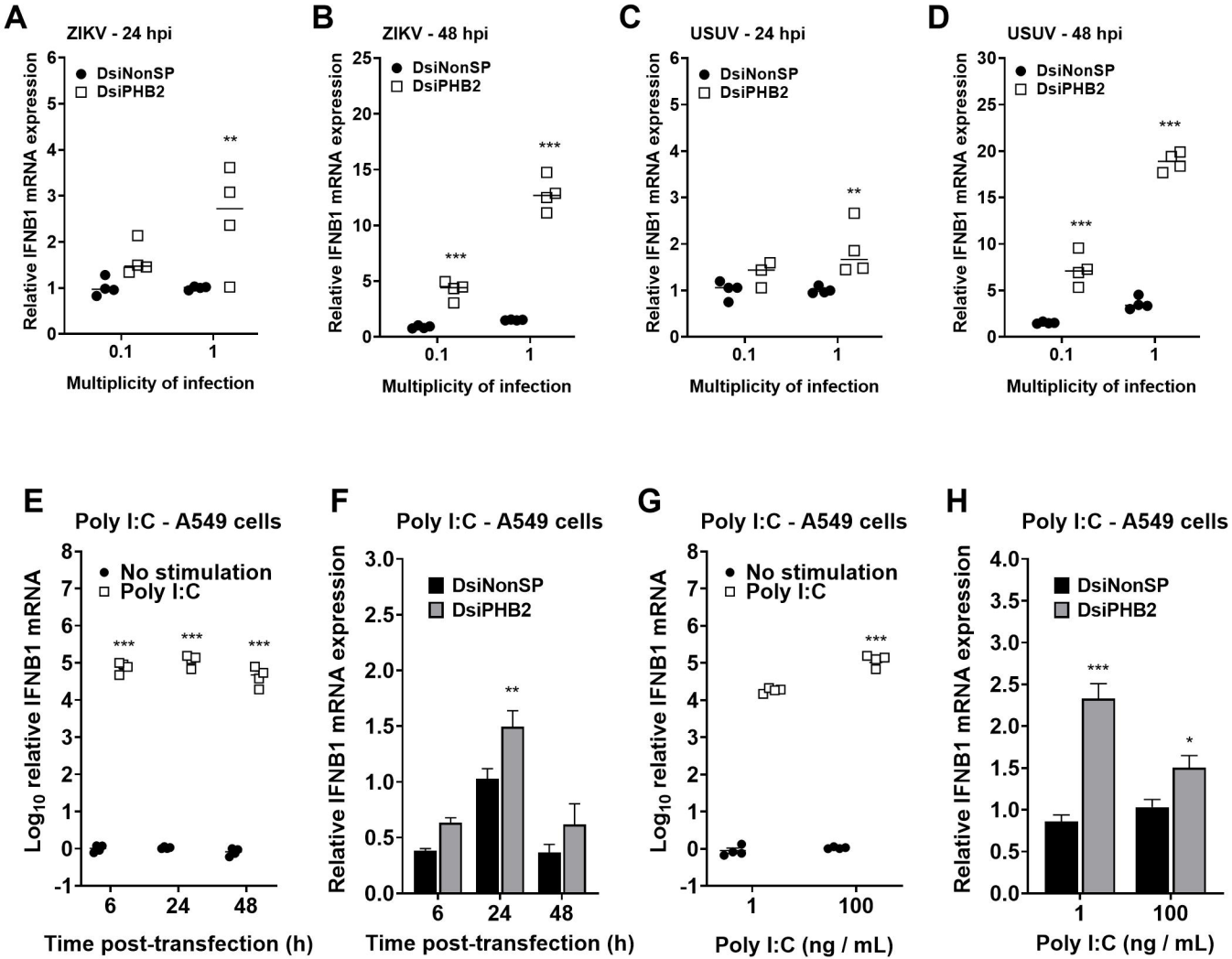
A
ZIKV - 24 hpi
DsiNonSP
DsiPHB2
Relative IFNB1 mRNA expression
Multiplicity of infection
B
ZIKV - 48 hpi
C
USUV - 24 hpi
D
USUV - 48 hpi
E
Poly I:C - A549 cells
No stimulation
Poly I:C
Log10 relative IFNB1 mRNA
Time post-transfection (h)
F
G
Poly I:C (ng / mL)
H

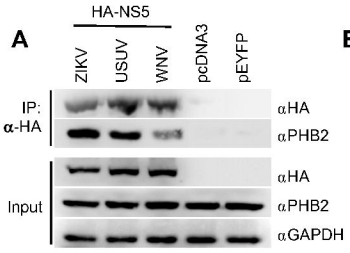
A
HA-NS5
ZIKV
USUV
WNV
pcDNA3
pEYFP
IP:
α-HA
αHA
αPHB2
Input
αHA
αPHB2
αGAPDH

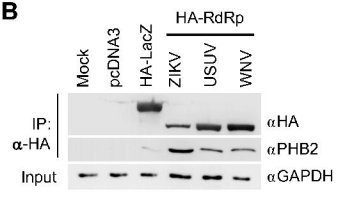
B
Mock
pcDNA3
HA-LacZ
HA-RdRp
ZIKV
USUV
WNV
IP:
α-HA
αHA
αPHB2
Input
αGAPDH

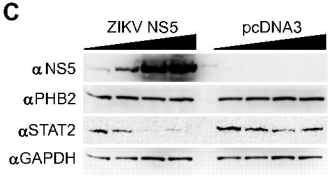
C
ZIKV NS5
pcDNA3
αNS5
αPHB2
αSTAT2
αGAPDH

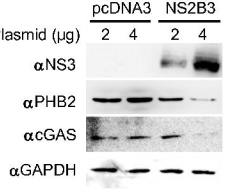
D
pcDNA3
NS2B3
Plasmid (μg)
2
4
2
4
αNS3
αPHB2
αcGAS
αGAPDH

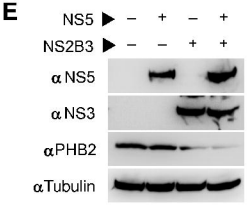
E
NS5
NS2B3
αNS5
αNS3
αPHB2
αTubulin

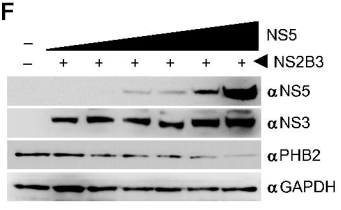
F
NS5
NS2B3
αNS5
αNS3
αPHB2
αGAPDH